Zur Homepage der Dissertation

Statistical Mechanics of Strongly Driven Ising Systems

Vom Fachbereich Physik der
Carl von Ossietzky Universität Oldenburg
zur Erlangung des Grades eines

Doktors der Naturwissenschaften

angenommene Dissertation.

Johannes Hausmann
geb. am 10. April 1968
in Freiburg im Breisgau

Erstreferent: Prof. Dr. P. Ruján
Zweitreferent: Prof. Dr. J.Peinke

Oldenburg, den 16. 10. 2001

Statistical Mechanics of Strongly Driven Ising Systems

Vom Fachbereich Physik der
Carl von Ossietzky Universität Oldenburg
zur Erlangung des Grades eines

Doktors der Naturwissenschaften

angenommene Dissertation.

Johannes Hausmann
geb. am 10. April 1968
in Freiburg im Breisgau

Erstreferent: Prof. Dr. P. Ruján
Zweitreferent: Prof. Dr. J.Peinke

Oldenburg, den 16. 10. 2001

Abstract

This work considers the behavior the Ising model of a ferromagnet subject to a strong, randomly switching external driving field. A formalism based on the master equation to handle such nonequilibrium systems is introduced and applied to a mean field approximation, and one- and two-dimensional variants of the model. A novel type of phase transition related to spontaneous symmetry breaking and dynamic freezing occurs which depends on the strength of the driving field. The complex analytic structure of the stationary magnetization distributions is shown to range from singular-continuous with euclidean or fractal support to all continuous. Analytic results are presented for the mean field and one-dimensional cases, whereas Monte-Carlo simulations provide insight into the two-dimensional model. Also, an interpretation of the model from a neurobiological point of view is given.

Diese Arbeit beschäftigt sich mit dem Verhalten des Ising-Modells eines Ferromagneten unter dem Einfluß eines starken, zufällig geschalteten externen Magnetfeldes. Ein auf der Master-Gleichung basierender Formalismus für Nicht-Gleichgewichts-Systeme wird eingeführt und auf eine Molekularfeldtheorie des Modells, sowie auf ein- und zwei-dimensionale Varianten angewendet. In Abhängigkeit von der Stärke des Antriebs tritt ein neuartiger Phasenübergang auf, der mit spontaner Symmetriebrechung und dynamischem Einfrieren in Zusammenhang steht. Die stationären Magnetisierungsverteilungen zeigen in weiten Bereichen des Phasendiagramms fraktale Eigenschaften. Für die Molekularfeldtheorie und den eindimensionalen Fall werden analytische Ergebnisse präsentiert, während für das zweidimensionale Modell auf Monte-Carlo-Simulationen zurückgegriffen werden muß. Abschließend wird auf eine neurobiologische Interpretation des Modells eingegangen.

‘So it’s false.’
‘What isn’t?’
‘Intellectual achievement. The exercise of skill. Human feeling.’
from Iain M. Banks, “The Player of Games”

Preface

In the fall of 1995, I was given the chance to work for one year with the neurocomputer SYNAPSE1/N110 of Fa. Siemens – without a clue as to what one might be able to do with it apart from simulating neural networks. The only condition was to present several applications to demonstrate the power of this machine. Neglecting the strong time constraint, I was in a situation that one would consider ideal for scientific work: A great infrastructure with respect to man and machine, as well as the freedom to pursue promising subjects I deemed interesting. It was during this time that the stage was set to take the first steps towards the work presented in the following chapters.

At this point, I would like to express my gratitude to my mentor, Prof. Dr. Pál Ruján, as well as to the other members of AG spÎn[1], Dr. Harry Urbschat and Thorsten Wanschura. Their democratic ways of “doing science” provide an atmosphere of friendship that procures the excitement and enjoyment of scientific work I have come to value in the past three and a half years. Also, thanks go to those involved with the proofreading. Next, I would like to thank Linus Torvalds for providing the computer community with Linux, one of the best computer operating systems around. And finally, I would like to thank my girlfriend for putting up with me all this time.

J.H.

[1]The Statistical Physics In the Neurosciences group at Carl von Ossietzky Universität Oldenburg

Contents

Chapter 1

Introduction

The original motivation to study the statistical mechanics of strongly driven, complex systems originates from several roots. First and foremost, there is the interplay between the curiosity of a physicist on one hand, and feasibility estimates on the other. Considering that fluid dynamics, climatology, or even the function of the human brain (which consists of around one hundred billion signal processing cells called neurons) might fall into this category, one can surmise the enormous hurdles that contemporary physics has yet to overcome, that is, feasibility is rather restrictive with respect to the choice of *interesting* problems one might investigate.

As a concrete example, one of the projects in SFB 517 “Neurokognition” has as its goal the understanding of the way information is coded by the retina, which transforms the optical images we perceive into electrical signals called spikes. It is these spikes that are further processed by the nerve cells of the brain, giving in the end rise to our sense of vision. It is generally accepted that a typical patch of cells processing spikes receives input signals following a Poisson distribution. From a statistical mechanics point of view, one would like to understand how “noise transformation” takes place in such a system of many, strongly connected units *driven by an external source of noise*. Of course, choosing a physical approach will involve an extreme simplification with respect to the complex nature of nerve tissue but there’s hope to learn something about the properties of such a model that may be transferred to the “real thing”.

From previous work of Pál Ruján[GyRu84] related to the so-called random field Ising model[BrAe83, AeBr83] stems the suggestion of an experiment that fits perfectly into this context. The idea is to take a simple, well-known model from statistical mechanics like the Ising ferromagnet and to drive it with a strong, random external magnetic field, thus creating a nonequilibrium situation. As the model lives on the border of dynamic systems theory, mostly concerned with few degrees of freedom, *and* statistical physics, it may interest the theorist how these two domains interact.

The subject of this work is the randomly driven Ising ferromagnet. The results presented in the following have been published in [HaRu97], [HaRu99a], and [HaRu99b]. In the remainder of this chapter, the model itself will be specified and put in relation to previous work. In Chapter 2, a theoretical framework is developed to handle this type of system. Next, in Chapter 3, the model is discussed in mean field approximation. Chapter 4 and 5 detail results for one and two dimensions, the former exact, the latter derived from Monte Carlo simulations. Then, an interpretation of the model in the above-mentioned neurobiological context is given in Chapter 6. Concluding remarks complete the work in Chapter 7.

1.1 The randomly driven Ising ferromagnet

This section serves to give a general idea of the model underlying the work in the following chapters, the randomly driven Ising ferromagnet (RDIM). Some of the typical quantities of interest are defined in the context of the well-known Ising model of a magnet in one dimension. Following this, the key concept of the random external driving field is explained. More details will follow in Chapter 2, and later on when required.

Consider a line of lattice sites numbered from $i = 1 \dots N$. At each site i, let there be a microscopic magnetic moment, or spin, pointing either parallel or antiparallel to some preferred direction. As usual, define a spin variable $s_i \in \{-1, +1\}$ for each site having two possible configurations. Configuration space thus consists of the set of 2^N corners of the N-dimensional hypercube defined on $[-1, 1] \otimes [-1, 1] \otimes \cdots \otimes [-1, 1]$.

In general, the energy of interaction of two magnetic moments is proportional to their dot product $\vec{\mu}_1 \cdot \vec{\mu}_2$. The presence of an external magnetic field $\vec{H}$ gives rise to an energy proportional to $\vec{\mu} \cdot \vec{H}$. Hence, the simplest choice of interactions between next neighbors and a global field defines the Hamiltonian

$$\mathcal{H} := -J\sum_{i=1}^{N} s_i s_{i+1} - H\sum_{i=1}^{N} s_i, \tag{1.1}$$

where J and H are global coupling constants, that is, the interactions are translation invariant. The model is called ferromagnetic if $J > 0$ or anti-ferromagnetic if $J < 0$.

The usual approach in equilibrium statistical mechanics provides the link from microscopic interactions defined by the above Hamiltonian to stationary thermodynamic properties by evaluating exactly or approximately the (in this case canonical) partition function

$$Z(T, H) := \sum_{\{C\}} e^{-\beta E[C]}, \tag{1.2}$$

where $\beta := \frac{1}{k_B T}$ with the Boltzmann constant k_B and the temperature T of the heat bath the system is in contact with. $\{C\}$ is the set of hypercube corners mentioned (or generally, the set of all possible configurations). If Z is available, one may calculate, for example, the free energy $\mathcal{F}$, the mean magnetization M, and the magnetic susceptibility χ,

$$\mathcal{F}(T, H) = -kT \ln Z \tag{1.3}$$

$$M(T, H) = -\frac{\partial}{\partial H} F(T, H) \tag{1.4}$$

$$\chi = \frac{\partial}{\partial H} M(T, H) \,|_{H=0}, \tag{1.5}$$

or any other thermodynamic quantity associated with the model. Typically, one performs the thermodynamic limit $N \mapsto \infty$ to describe macroscopic systems. This completes the description of equilibrium stationary states of statistical physical models. It is the calculation of Z that most often proves to be a highly nontrivial matter[1].

The key component of the RDIM distinguishing it from previous work is the dynamics of the external driving field. If this dynamics is slow in the sense that the system remains near global equilibrium at all times, the usual methods may be adapted to still correctly describe it. This is not the case for a field changing fast in comparison with relaxation to global

[1] except for the simplest of models like the one defined by Eq. 1.1

equilibrium. A driving field $H(t)$ governed by a *fast* chaotic or stochastic dynamics prohibits the normal evolution towards a Boltzmann distribution of states. Adjusting the time scale of the field *below* the system's relaxation time leads to competition between two objectives defined by the Hamiltonian, Eq. 1.1: Try to achieve local equilibrium on one hand, but follow the driving field on the other hand. Before some of the properties of the nonequilibrium stationary states of the RDIM are analyzed, the stage is set in the next section with an overview of related work.

1.2 What's been done

Due to the time-dependent external driving field, the RDIM is a dynamic system. It is also a statistical physics model, as it possesses a macroscopic number of degrees of freedom.

Coming from the theory of dynamic systems, there are several recent articles concerned with many body problems. In [SiSz96], Simányi and Szász prove the Boltzmann-Sinai ergodic hypothesis for a system of $N \geq 2$ hard balls of mass m_i for $i = 1 \ldots N$ for almost every distribution of masses. The balls move uniformly on a ν-dimensional torus ($\nu \geq 3$) and interact through elastic collisions. Gallavotti and Cohen [GaCo95a] discuss the application of a principle similar to the ergodic hypothesis to a many-particle model of a strongly sheared fluid, deriving results on the (macroscopic) entropy production fluctuations. In [GaCo95b], they develop this idea into the *chaotic hypothesis* for reversible, dissipative many-particle systems in a nonequilibrium stationary state, which allows one to derive macroscopic properties of such systems.

A model closely related to the RDIM is the random field Ising model (RFIM), first introduced by [BrAe83]. Its Hamiltonian is modified with respect to Eq.1.1 by allowing for a binary random field H_i instead of the global field H, that is, at each site i of the chain there is an external field $H_i = H_0$ with probability p and $H_i = -H_0$ with probability $1 - p$, respectively:

$$\mathcal{H} := -J \sum_{i=1}^{N} s_i s_{i+1} - \sum_{i=1}^{N} H_i s_i, \tag{1.6}$$

It is still a static model as the random field is quenched. Nonetheless, there are qualitative similarities to the RDIM, for example, the integrated probability distribution is a devil´s staircase [BrAe83, AeBr83]. In [Ru78], it was shown that the problem may be reduced to a single spin in a local field governed by a discrete map. In the case of the RFIM, the map is stochastic, leading to an invariant measure with possibly fractal support due to the existence of a strange attractor for the (random) local field. Quantities like the free energy or Edwards-Anderson parameter thus must be calculated using a fractal measure [GyRu84]. Furthermore, the multifractal spectrum of this measure may be determined [Ev87] and its relation to free energy fluctuations [BeSz88] established. An alternate view of the strange attractor as the repellor of the backward iteration of the inverse map [SzBe87] leads to a generalized eigenvalue equation from which generalized dimensions of the measure may be calculated [Be89]. Many of the methods developed for this model may be transferred to the RDIM.

More recently, attention has been focused on the Ising ferromagnet in a time-dependent, sinusoidal external field. The phenomenon of interest here is magnetic hysteresis. In [RaKr90], a detailed study of the cubic $O(N)$-model in the $N \mapsto \infty$ limit is presented. The evolution of the shapes of hysteretic loops depends on the strength of the external field and on its frequency, leading to five types of loops. Their area shows a scaling behavior described by $A \sim H_0^\alpha \Omega^\beta$ with $\alpha \approx 0.66$ and $\beta \approx 0.33$ for low values of H_0 and Ω, corresponding to the first three loop types. The mean field kinetic Ising model in a sinusoidal field shows a dynamic phase transition related to the symmetry of solutions [ToOl90]. For a strong field/high temperature, the stationary solution is symmetric in the sense $m(t + \frac{\tau}{2}) = -m(t)$. As the time-averaged magnetization m is zero, this phase is called paramagnetic. Conversely, in a weak field/low temperature situation, m oscillates around a non-zero mean, leading to a ferromagnetic phase. An analysis of the stability of these solutions shows that there exists an area in the $H - T$-phase diagram where the para- and ferromagnetic phases overlap, and there exists a tricritical point. Monte Carlo simulations of the 2D kinetic Ising model [LoPe90] and cell-dynamical simulations [SeMa92] confirm the dynamic phase transition and indicate scaling behavior, but not the existence of the tricritical point. Further Monte Carlo studies [SiRa96] show that the response of an Ising system depends on the decay mechanism of the metastable states. The lifetimes of latter were previously shown to depend on system size, temperature, and (exponentially on the inverse) strength of the unfavorable field using droplet theory and Monte Carlo simulations [RiTo94].

M. Accharyya has followed an approach very similar to the RDIM in [Ac98]. 2D Monte Carlo simulations and numerical integration of a mean field Ising model in a random field with a uniform distribution on a given interval show a (continuous) nonequilibrium phase transition. It is related to dynamical symmetry breaking of the time-averaged magnetization. Details on this paper will be presented in the appropriate sections.

Turning to an experimental view, much progress has been made in the past few years to handle ultrathin magnetic films. In [BaBr89], the magnetic aftereffect of Co films (0.4 to 2.0 nm thick) is investigated. Magnetization reversal seems to occur due to domain wall motion as opposed to the reversal of independent particles. In [PoMe90], the time development of magnetic domains in a similar experiment was visualized using a magneto-optic microscope. Reversal is dominated by nucleation or wall motion depending on the sample and the strength of the field. The formation of magnetic domains is studied in [AlSt90] where it is found that there is a transition from out-of-plane to in-plane magnetization as the thickness of a Co film is increased. Also, the size of domains depends linearly on sample thickness. The scaling law for the area of the hysteretic loop is confirmed for Fe films of a few monolayers using the magneto-optic Kerr-effect in [HeWa93]. These experiments indicate that ultrathin ferromagnetic films indeed belong to a dynamic Ising universality class. The current state of experimental techniques is such that a verification of the effects seen in the RDIM seems to be in reach.

Hopefully this brief introduction of the randomly driven Ising model and the background scene surrounding it will suffice to persuade the reader that the investigation of its properties proves to be highly interesting. The next chapter introduces a general formalism designed to handle a system of spins in a nonequilibrium situation. It is based on the Master equation for the time-dependent probability distribution of a system of spins.

Chapter 2

Formalism

This chapter is devoted to the introduction of a theoretical formalism to describe the behavior of a statistical mechanical spin model driven by a time-dependent external magnetic field. In the first section, the basic assumptions necessary to start the analysis are presented. In the second section, simplifications are made using a random, dichotomic driving field, leading to a discrete "coarse-grained" Master equation. Thirdly, one needs to define quantities from dynamical systems theory to describe the stationary properties and the dynamical aspects of the model.

2.1 The Master equation

We will discuss a system of spins $\vec{\mu} = (s_1, s_2, \ldots, s_N)$, $s_i = \pm 1$ for $i = 1, \ldots, N$, in contact with a thermal heat bath, envisioning the later as the result of spin interactions with phonons. Assume now that the evolution of this system is completely described by a joint probability distribution $|P(\{s_i\}, t)\rangle$ subject to the Master equation

$$\partial_t |P(\{s_i\}, t)\rangle = -\hat{\mathcal{L}}_{B(t)} |P(\{s_i\}, t)\rangle \tag{2.1}$$

where $\hat{\mathcal{L}}_{B(t)}$ is the Liouville operator describing the probability flow into and out of the probability of states $\vec{\mu}$ if the system is subject to an external magnetic field $B(t)$ at time t. Note that in general, $[\hat{\mathcal{L}}_B, \hat{\mathcal{L}}_{B'}] \neq 0$ for $B \neq B'$. The ket $|P\rangle$ indicates that we have a choice of bases to describe the distribution.

2.1.1 Spin configuration and spin product basis

The obvious choice is the *spin configuration basis* in which $|P\rangle$ is expressed using $P(\vec{\mu}, t)$ for each $\vec{\mu}$ in the set of all 2^N possible configurations $\{s_i\}$. Hence we have

$$\vec{P}(t) = (P(\vec{\mu}^{(1)}, t), P(\vec{\mu}^{(2)}, t), \ldots, P(\vec{\mu}^{(2^N)}, t))^T \tag{2.2}$$

with $P(\vec{\mu}^{(i)}, t)$ denoting the probability of the i-th spin configuration at time t. An alternate expression of $|P\rangle$ in the *space of spin products* is given by

$$P(\{s_i\}, t) = \frac{1}{2^N}\left(1 + \sum_{i=1}^{N} m_i(t)s_i + \sum_{i<j}^{N} c_{i,j}(t)s_is_j + \cdots + c_{1,2,\ldots,N}(t)s_1s_2\ldots s_N\right)$$

where $m_i(t) := \sum_{\{s_i\}} s_iP(\{s_i\}, t)$ is the average local magnetization of spin i at time t, $c_{i,j}$ the two-spin correlation between spins i and j, and so forth[1]. Introducing the 2^N index sets α obvious from the last equation and defining the averages of all products of spins $\pi_\alpha(t) = \langle\prod_{j\in\alpha} s_j\rangle = \sum_{\{s_i\}} P(\{s_i\}, t)\prod_{j\in\alpha} s_j$ this may be written more compactly as

$$P(\{s_i\}, t) = \frac{1}{2^N}\left(\sum_{\alpha=1}^{2^N} \pi_\alpha(t)\prod_{j\in\alpha} s_j\right).$$

In this basis $|P(t)\rangle$ may be expressed as

$$\vec{\pi}(t) = \frac{1}{2^N}(1, \langle s_1\rangle_t, \langle s_2\rangle_t, \ldots, \langle s_N\rangle_t, \langle s_1s_2\rangle_t, \ldots, \langle s_1s_2\cdots s_N\rangle_t)^T \tag{2.3}$$

where $\langle\cdot\rangle_t$ is the thermal average at time t. Thus in both cases, $|P\rangle$ may be expressed as a 2^N-dimensional vector[2], and the action of the Liouville operator may be expressed in matrix form.

2.1.2 Some properties of $\hat{\mathcal{L}}$

Keeping in mind the first representation (2.2), we can say the following on the eigenvalues of $\mathcal{L}_{ij}$. As the components of $\vec{P}$ are the probabilities of spin

[1]This representation is a generalization to N dimensions of the fact that *any* spin function can be parameterized as $f(s_1, s_2) = a + bs_1 + cs_2 + ds_1s_2$, where $s_1, s_2 \in \{-1, +1\}$.

[2]Normalized with respect to the L^1 norm

configurations, its evolution is described by

$$\vec{P}(t+\Delta t) := \mathcal{M}\vec{P}(t) \tag{2.4}$$

where $\mathcal{M}$ must be a stochastic matrix[3]. The definition of the Liouville operator is

$$\vec{P}(t+\Delta t) - \vec{P}(t) = (\mathcal{M}-\mathcal{E})\vec{P}(t) =: -\Delta t \mathcal{L}\vec{P}(t), \tag{2.5}$$

where $\mathcal{E}$ is the unit matrix. From the characteristic polynomial of $\mathcal{M}$ we gather

$$\begin{aligned} \prod_{i=0}^{2^N-1}(\mu-\mu_i) &= \det(\mathcal{M}-\mathcal{E}+\mathcal{E}-\mu\mathcal{E}) & (2.6)\\ &= \det(-\Delta t\mathcal{L}-(\mu-1)\mathcal{E}) =: \det(\Delta t\mathcal{L}-\lambda\mathcal{E}), & (2.7) \end{aligned}$$

so if we know the eigenvalues of $\mathcal{M}$ we also know those of $\mathcal{L}$, and vice versa. From the stochasticity property we immediately figure

$$\begin{aligned} (1,1,\ldots,1)\mathcal{M} &= 1\cdot(1,1,\ldots,1), & (2.8)\\ \text{and } (1,1,\ldots,1)\mathcal{L} &= 0\cdot(1,1,\ldots,1). & (2.9) \end{aligned}$$

Therefore $(1,1,\ldots,1)$ is a left eigenvector of $\hat{\mathcal{L}}$ for eigenvalue $\lambda_0 = 0$, or generally, $\lambda_i \sim 1-\mu_i$. The operator $\hat{\mathcal{L}}$ is not necessarily symmetric, but it may be expanded in a biorthogonal basis of its left and right eigenvectors $\langle l_n|r_n\rangle = a\delta_{n,m}$, respectively:

$$\hat{\mathcal{L}} = \frac{1}{a}\sum_{n=0}^{2^N-1}|r_n\rangle\lambda_n\langle l_n|. \tag{2.10}$$

Like in quantum mechanics, functions of $\hat{\mathcal{L}}$ may be expressed via series expansions, $f(\mathcal{L}) = \frac{1}{a}\sum_{n=0}^{2^N-1}|r_n\rangle f(\lambda_n)\langle l_n|$. For a constant external field, the formal solution of the Master equation then is

$$|P(t)\rangle = \exp(-t\hat{\mathcal{L}})|P(0)\rangle = \frac{1}{a}\sum_{n=0}^{2^N-1}|r_n\rangle e^{-\lambda_n t}\langle l_n|P(0)\rangle, \tag{2.11}$$

where $|P(0)\rangle$ is the state of the system at $t=0$ (consistent with whatever macroscopic constraints there are). Ordering the eigenvalues $\lambda_0 = 0 \le \lambda_1 \le$

[3] $\forall i,j: 0 \le \mathcal{M}_{ij} \le 1$ and $\forall j: \sum_i \mathcal{M}_{ij} = 1$. All its eigenvalues are real and ≤ 1.

$\cdots \leq \lambda_{2^N-1}$, we see that Eq. (2.11) describes the system´s relaxation towards global thermal equilibrium[4],

$$|P_{eq}\rangle = \lim_{t\mapsto\infty} |P(t)\rangle = \frac{1}{a}|r_0\rangle. \tag{2.12}$$

Thus the components of $|r_0\rangle$ in the spin configuration basis are the Boltzmann factors e^{-E/k_BT}, and its L^1-norm $\langle l_0|r_0\rangle \equiv a = \sum_{\{s_i\}} e^{-E/k_BT} = Z$ yields the stationary canonical partition function. Note that the L^2-norm of $|P(t)\rangle$ is

$$\begin{aligned}\langle P(t)|P(t)\rangle &= \frac{1}{Z^2}\sum_{n,m}\langle P(0)|r_n\rangle e^{-t\lambda_n}\langle l_n|r_m\rangle e^{-t\lambda_m}\langle l_m|P(0)\rangle && (2.13)\\ &= \frac{1}{Z}\sum_{n} e^{-2t\lambda_n}\langle P(0)|r_n\rangle\langle l_n|P(0)\rangle. && (2.14)\end{aligned}$$

Hence, if the system is in a state $|P(0)\rangle = \sum_n \alpha_n|r_n\rangle$ (with the corresponding bra $\langle P(0)| = \sum_m \beta_m\langle l_m|$),

$$\lim_{t\mapsto\infty}\langle P(t)|P(t)\rangle = \frac{1}{Z}\sum_n \langle l_0|r_0\rangle\langle l_0|r_0\rangle\alpha_0\beta_0 = Z\alpha_0\beta_0. \tag{2.15}$$

Turning back to a time-dependent field, there are three characteristic time scales of interest: That of spin-phonon interactions τ_{flip}, the slowest relaxation mode of the system as a whole, $\tau_{sys} = \lambda_1^{-1}$, and τ_B describing the field dynamics. Assuming $\tau_{flip} \ll \tau_{sys} \ll \tau_B$, i.e. a slowly changing magnetic field, the system is always in local *and* global thermal equilibrium on the field´s time scale. It´s a different story if we do not permit this relaxation by rapidly switching the field. If $\tau_{flip} \ll \tau_B \ll \tau_{sys}$ the system remains in local equilibrium, but it does not have the time to reach global equilibrium.

2.2 Driving field distribution and discrete Master Equation

As mentioned in the introduction, the external driving field might be a random variable or subject to a chaotic dynamics. In the following, it is sampled

[4] If we ignore the possibility that $\mathcal{L}$ is degenerate!

identically and independently from a distribution $\rho(B)$. Furthermore, the field is constant during time intervals of length τ_B,

$$B(t) = B\rho(B)\sum_{n=0}^{\infty}\Theta(t - n\tau_B)\Theta((n+1)\tau_b - t). \tag{2.16}$$

As before, the Master Eq. (2.1) can be integrated exactly for the time intervals during which the field is constant,$t_{n-1} < t < t_n$:

$$|P(t)\rangle = \exp(-(t - t_{n-1})\hat{\mathcal{L}}_{B(t_{n-1})})|P(t_{n-1})\rangle. \tag{2.17}$$

For $t := \lim_{\epsilon\mapsto 0}(t_n - \epsilon)$ we see

$$|P(t_n)\rangle = \exp(-\tau_B\hat{\mathcal{L}}_{B(t_{n-1})})|P(t_{n-1})\rangle = \widehat{\mathcal{M}}^{\tau_B}_{B(t_{n-1})}|P(t_{n-1})\rangle. \tag{2.18}$$

2.2.1 Coarse-graining the Master Equation

Focusing on the case of a rapidly switching field, $\tau_B \ll \tau_{sys}$ or $\lambda_1\tau_B \ll 1$, Eq. (2.18) may be approximated by expanding the exponential to first order giving

$$|P(t_n)\rangle \approx (\mathcal{E} - \tau_B\hat{\mathcal{L}}_{B(t_{n-1})})|P(t_{n-1})\rangle. \tag{2.19}$$

Eq. (2.19) may be rewritten as

$$\frac{|P(t_n)\rangle - |P(t_{n-1})\rangle}{\tau_B} \approx -\hat{\mathcal{L}}_{B(t_{n-1})}|P(t_{n-1})\rangle, \tag{2.20}$$

which is the "coarse-grained" Master Equation announced at the beginning of this chapter. Of course, it only describes correctly the long term behavior of Eq. (2.19) due to those eigenvalues of $\hat{\mathcal{L}}$ that satisfy $\lambda_i\tau_B \ll 1$. At time scale τ_B, the short term effects due to the larger eigenvalues may be considered to have already relaxed. They are not taken into further account. The approximated form Eq. (2.20) defines a discrete dynamics for the evolution of the probability distribution $|P(t_n)\rangle$. It is this dynamics that we will investigate in the following chapters.

2.2.2 An iterated function system

To further simplify things, restrict the external driving field distribution to a symmetric, binary-valued one,

$$\rho(B) = \frac{1}{2}\delta(B - B_0) + \frac{1}{2}\delta(B + B_0). \tag{2.21}$$

This choice leads to the iterated function systems (IFSs)[5] developed by Barnsley and Demko [BaDe85]. Thinking again in terms of matrices, the original problem Eq. (2.1) is now transformed to the action of two maps, $f_{+/-}(\vec{P}) := \mathcal{M}_{+/-}^{\tau_B}\vec{P}$ on a (normalized) vector $\vec{P}$. A trajectory is given by choosing at random a sequence of signs $+$ or $-$ and applying the corresponding map $f_{+/-}$. The stationary properties of the RDIM will thus be closely linked to those of the attractor of the associated IFS. Many of the results coming from the mathematics of fractals [Ma77] apply to the RDIM, as will become clear in the next chapter.

2.3 Stationary and dynamical properties

In order to make sensible statements about the nonequilibrium stationary states of the RDIM, several concepts from the theory of dynamical systems should be mentioned.

An important object in dynamical systems is the invariant measure induced by a dynamics[6], in our case the Master Equation (2.20) (see, for example, [ChWr81]). In the spin product basis, denote by $\mathcal{P}_s(\vec{\pi})$ the stationary probability distribution induced by (2.20). It has to satisfy a self consistency relation called the Chapman-Kolmogorov equation:

$$\mathcal{P}_s(\vec{\pi}) = \int d\vec{\nu} \int dB \delta[\vec{\pi} - \exp(-\mathcal{L}_B \tau_B)\vec{\nu}]\rho(B)\mathcal{P}_s(\vec{\nu}) =: \widetilde{\mathcal{K}}\mathcal{P}_s(\vec{\pi}), \qquad (2.22)$$

where $\vec{\nu}$ is also in the spin product representation. $\widetilde{\mathcal{K}}$ is called Frobenius-Perron operator. The meaning of Eq. (2.22) is that the probability of state $\vec{\pi}$ has to be invariant when subject to the dynamics Eq. (2.18). The contribution to this probability of a state $\vec{\nu}$ that maps into $\vec{\pi}$ when the field is B

[5]Recall, for example, the famous middle third Cantor set. The associated IFS comprises of two linear functions mapping the unit interval to $[0, \frac{1}{3}] \cup [\frac{2}{3}, 1]$. The resulting set is then iteratively mapped, leading in the limit of infinitely many iterations to "fractal dust", the Cantor set. This "dust" is rather peculiar: On one hand, its Lebesgue measure is zero, but on the other hand, it is much "fatter" than the (countably infinite) set of rational numbers in the unit interval. This led to the development of a generalized concept of dimension related to measure theory. Fractal sets are commonly associated with non-integer dimension, for example, the Cantor set has Hausdorff dimension $d_F = \frac{\ln 2}{\ln 3}$. A good mathematical introduction is given by Kenneth Falconer [Fa90].

[6]If the dynamics is characterized by a mapping $f : D \mapsto D$, a measure μ on D is called invariant if for every subset $A \subset D : \mu(f^{-1}(A)) = \mu(A)$ holds.

is $\rho(B)\mathcal{P}_s(\vec{\nu})$. Those states that do not map into $\vec{\pi}$ are filtered out by the Dirac-δ. The sum of all contributions, i.e. the integral in the above equation, must be $\mathcal{P}_s(\vec{\pi})$.

The calculation of the nonequilibrium stationary value of some spin observable $A(\vec{\pi})$ thus requires a thermal $\langle\cdot\rangle$ *and* a dynamic average $[\cdot]$,

$$\overline{A(\vec{\pi})} = [\langle A\rangle] = \int d\vec{\nu} \int dB \delta[\vec{\pi} - \exp(-\mathcal{L}_B \tau_B)\vec{\nu}] A(\vec{\nu})\rho(B)\mathcal{P}_s(\vec{\nu}). \tag{2.23}$$

An interesting question is *how* a randomly driven system like the RDIM relaxes to its stationary state. To assess this, one would have to solve the right eigenvalue problem of the Frobenius-Perron operator introduced above,

$$\widetilde{\mathcal{K}}\mathcal{R}_m = \kappa_m \mathcal{R}_m. \tag{2.24}$$

The largest eigenvalue must be $\kappa_0 = 1$, which is associated with the stationary distribution $\mathcal{R}_0 \equiv \mathcal{P}_s$.

The formalism outlined this far seems quite involved and the question arises if it can be successfully applied to a physical system. As already indicated, further discussions will be limited to a spin system in a random, dichotomic external field. The next chapter shows that indeed a mean field theory can be developed that leads to some surprising results.

Chapter 3

Mean Field Approximation

In order to legitimate the formalism developed in the last chapter, we will consider now a mean field theory of the RDIM. Similar to the zero-field mean field Ising model, there is a transition from a paramagnetic phase to a ferromagnetic one. The dependence on temperature and the strength of the external field, though, is *not* what one would expect following the conventional statistical physics approach. Instead, the transition is related to a dynamic freezing of the system. To show these results, a mean field map is introduced in the next section. The phase transition is then calculated in the usual fashion. Next, this result is contrasted with a geometric interpretation of what is happening, followed by an explanation of the freezing process. A discussion of the multifractal regime rounds up the picture. Finally, a note on the character of the driving field is due.

3.1 The mean field map

As usual, the mean field Ising model is constructed by considering the thermodynamic limit of an N-dimensional simplex where all spins are next neighbors. The (extensive) energy then is

$$E = -\frac{J}{N}\sum_{i\neq j}^{N} s_i s_j - \mu_B B(t)\sum_{i=1}^{N} s_i. \tag{3.1}$$

Here, μ_B is the Bohr magneton and the external field $B(t)$ is given by Eq. (2.16) with the binary distribution Eq. (2.21). For a state $\vec{\mu}$, define

$\vec{\mu}_i := (s_1, s_2, \ldots, -s_i, \ldots, s_N)$. The Liouville operator may be represented using the well-known Glauber transition rate[Gl63]

$$w(\vec{\mu}_i|\vec{\mu}) = \frac{1}{2\alpha}\left(1 - s_i \tanh\left(\frac{K}{N}\sum_{j\neq i}^{N} s_j + H\right)\right), \tag{3.2}$$

where $K := \frac{J}{k_B T} =: \beta J$ and $H := \beta\mu_B B$ and α sets the time scale. Eq. (2.20) now leads to the following equation in the spin configuration basis:

$$P(\vec{\mu}, t+\tau_B) - P(\vec{\mu}, t) = \tau_B\left(\sum_{i=1}^{N} w(\vec{\mu}|\vec{\mu}_i)P(\vec{\mu}_i, t) - P(\vec{\mu}, t)\sum_{i=1}^{N} w(\vec{\mu}_i|\vec{\mu})\right).$$

Defining the average magnetization $m(t) := \frac{1}{N}\sum_{i=1}^{N} s_i(t) \in [-1, 1]$, one recovers in the thermodynamic limit $N \mapsto \infty$ the usual result

$$m(t+1) = \tanh(Km(t) + H(t)). \tag{3.3}$$

Here time is measured in units of $\alpha = \tau_B$. Due to the driving field distribution (2.21), this is a stochastic map,

$$m(t+1) = \begin{cases} \tanh(Km(t) + H_0) & \text{with probability } \frac{1}{2} \\ \tanh(Km(t) - H_0) & \text{with probability } \frac{1}{2} \end{cases} \tag{3.4}$$

with $H_0 := \beta\mu_B B_0$. This map is the basis for the investigation in the following sections.

3.2 The stationary phase diagram

This section first presents the standard expansion of moments of the dynamic average magnetization. It implies a relation between K and H_0 that describes the transition of the RDIM from para- to ferromagnetic behavior. Then, the mean field map is interpreted from a geometrical point of view related to the fixed points of the map's branches, which leads to an alternate approach to the phase diagram yielding a *different* critical field. It turns out that the phase transition is *not* continuous, but that $[m]$ jumps at a critical value of the driving field.

3.2.1 Expansion of moments

Due to the fact that the dynamic average of moments of the magnetization is constant in the stationary state, $[m^k(t+1)] = [m^k(t)]$,

$$[m^k(t)] = \left[\left(\frac{v+h}{1+vh} \right)^k \right], \tag{3.5}$$

where $v := \tanh(Km(t))$ and $h := \tanh(H(t))$. In the conventional approach, one assumes that the free energy of the system is analytic in $[m]$. Then Eq. (3.5) for $k = 1$ may be expanded in terms of the k-th moments of $[m]$ and h:

$$\begin{aligned}
[m] = \Bigg[\bigg(& Km(t) - \frac{1}{3}(Km(t))^3 + \frac{2}{15}(Km(t))^5 - \cdots + h \bigg) \\
& \times \left(1 - \left\{ Km(t) - \frac{1}{3}(Km(t))^3 + \frac{2}{15}(Km(t))^5 - \ldots \right\} h \right. \\
& \left. + \left\{ Km(t) - \frac{1}{3}(Km(t))^3 + \frac{2}{15}(Km(t))^5 - \ldots \right\}^2 h^2 - \ldots \right) \Bigg].
\end{aligned} \tag{3.6}$$

Thus

$$\begin{aligned}
[m] = {} & K[m] + [h] - K^2[m^2][h] - K[m][h^2] \\
& + K^3[m^3][h^2] + K^2[m^2][h^3] - \frac{1}{3}K^3[m^3] + \ldots
\end{aligned} \tag{3.7}$$

From similar expressions for higher odd moments one obtains $[m^k] = \mathcal{O}([h^{2k}])$. Noting that odd functions of h vanish in the dynamic average due to the symmetry of the field distribution, the first order expansion of $[m]$ in h^2 leads to

$$[m] \approx K(1 - \tanh^2(H_0))[m]. \tag{3.8}$$

The critical driving field, as a function of temperature, is given by

$$1 = K(1 - \tanh^2(H_0)) \tag{3.9}$$

$$\Rightarrow H_c = \frac{1}{2} \ln \left(\frac{1+m^\dagger}{1-m^\dagger} \right), \tag{3.10}$$

with $m^\dagger := \sqrt{\frac{K-1}{K}}$ for $K \geq 1$. As expected, in the absence of a driving field, $H_c = 0$, the result for the critical temperature $K_c = 1$ is consistent with the standard mean field result. With a bit of patience, higher order expansions may be obtained in the same way, as well as expressions for higher moments of the magnetization (see also [HaRu99a]).

3.2.2 Geometric analysis

Turning now to a geometric view, consider the stochastic map Eq. (3.4) shown in Fig. 3.1 for $K = 2$, $\frac{H_0}{K} = 0.5$. To generate a trajectory we have to chose a sequence of signs + and −, i.i.d. with $p_+ = p_- = \frac{1}{2}$, describing the sign of the external driving field, in accordance with (2.21). Starting from an arbitrary initial value $m(0) \equiv m_0 \in [-1, 1]$, the sequence prescribes which branch $f_+(m) := \tanh(Km + H_0)$ **or** $f_-(m) := \tanh(Km - H_0)$ of the map to take in the next time step, $m(t+1) = f_+(m(t))$ or $m(t+1) = f_-(m(t))$. Note that each branch has a (stable) fixed point $f_+(m_1) = m_1$ and $f_-(-m_1) = -m_1$, respectively. For example, a sequence consisting only of + signs leads to

$$\forall m_0 \in [-1, 1] : \lim_{t \mapsto \infty} f_+^{(t)}(m_0) = m_1 \tag{3.11}$$

with $f_+^{(1)}(m_0) := f_+(m_0)$ and $f_+^{(t)}(m) := f_+(f_+^{(t-1)}(m))$. This trajectory is indicated by the arrows in Fig. 3.1. Note that no matter how close to a fixed point of one branch a trajectory is, say m_1, it can always move *away* from it along the other branch, in this case f_-. Thus one may think of the dynamics as the competition between the two fixed points of the map.

3.2.3 An alternate approach to the phase diagram

In order to derive a phase diagram in the K-$\frac{H_0}{K}$-plane, one needs to analyze the behavior of the fixed points as functions of K and H_0. Fig. 3.2 shows that the upper branch f_+ has one, two, or three fixed points $m_1 \geq m_2 \geq m_3$. The arrows on the branches indicate in which direction points are mapped. The symmetry of tanh implies that $-m_1 \leq -m_2 \leq -m_3$ are the fixed points of f_-.

At high temperatures $K \leq 1$, $m_1 = m_2 = m_3$, independent of the field[1] H_0. An example is presented in Fig. 3.3. Due to the symmetry of the driving field distribution and the fact that a trajectory cannot be trapped near a fixed point, the dynamic averaged magnetization is $[m] = 0$. Hence,

[1]This is simply a property of $f : \mathbb{R} \mapsto [-1, 1], x \mapsto \tanh(x)$.

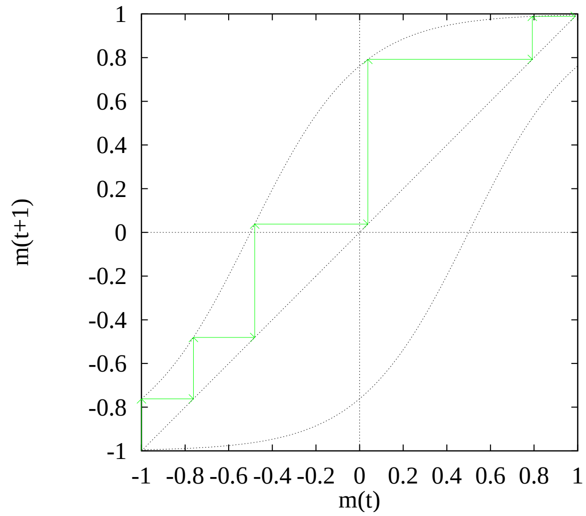

Figure 3.1: Upper and lower branches f_+ and f_- of the mean field map for $K = 2.0$ and $\frac{H_0}{K} = 0.5$. The arrows indicate the motion of $m_0 = -1$ subject to iteration along the upper branch.

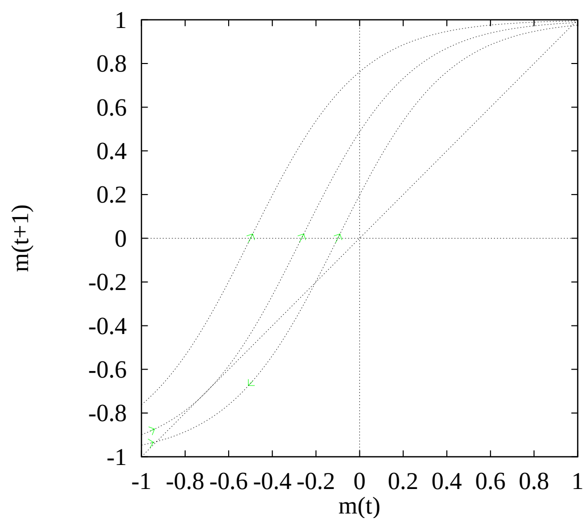

Figure 3.2: Upper branch f_+ of the mean field map for $K = 2$ and driving field strengths $\frac{H_0}{K} = 0.5$, 0.266, and 0.1 (from left to right). The arrows on each branch show in which direction points are mapped.

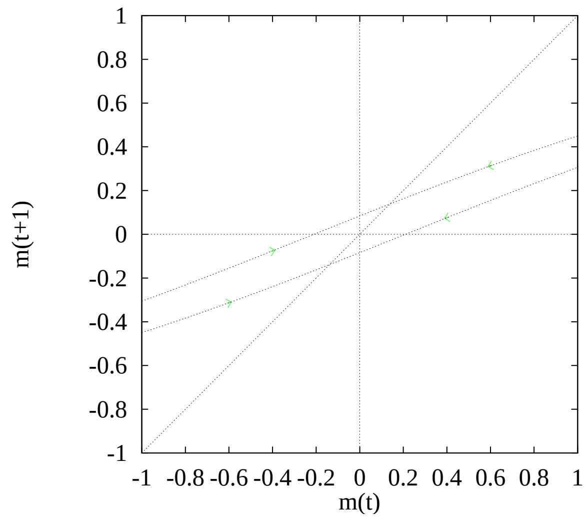

Figure 3.3: Mean field map for $K = 0.4$ and $\frac{H_0}{K} = 0.21$. The system is in the paramagnetic phase.

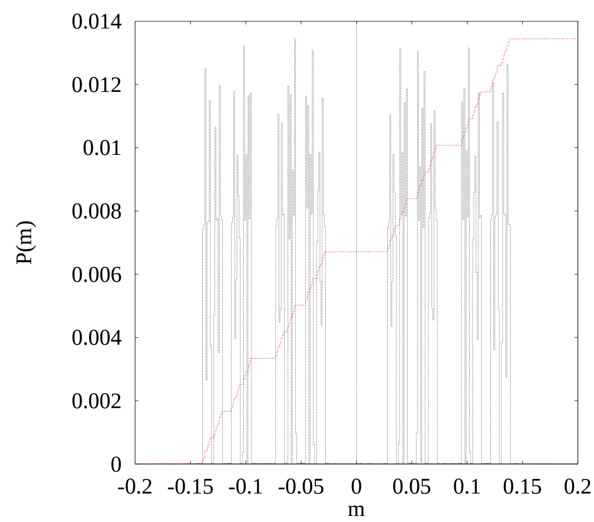

Figure 3.4: Stationary magnetization distribution of the map Fig. 3.3, $K = 0.4$ and $\frac{H_0}{K} = 0.21$. The integrated distribution, scaled to fit in the graph,is shown in red.

the system is in a *paramagnetic* phase. Fig. 3.4 displays the approximate stationary magnetization distribution $P(m)$. It was computed by tracking the evolution of 1000 initial values m_0 uniformly distributed in the interval $[-1, 1]$ for five thousand iterations[2] of the map Eq. (3.4). The stationary dynamics is confined to the interval $[-m_1, m_1]$. Note the well-separated peaks and the devil's staircase structure of the integrated distribution (the latter shown in red).

For low temperature $K > 1$, the slope of $\tanh(Km)$ at $m = 0$ for the first time becomes greater than the slope of the diagonal $m(t+1) = m(t)$, thus permitting $m_1 > m_2 > m_3$. From Fig. 3.2 it is obvious that this situation occurs for small driving fields. Note that m_2 is unstable, i.e. all points to the left of m_2 are mapped towards m_3 and all to the right of m_2 are mapped towards m_1 along the upper branch. Taking into account *both* branches, it is immediately clear from Fig. 3.5 that all $m > m_2$ are mapped towards m_1 *regardless* of whether f_+ or f_- is chosen. The same is true for all $m < -m_2$, which are mapped towards $-m_1$. Due to the stochastic nature of the driving field, all initial values $m \in [-m_2, m_2]$ will be eventually mapped outside this interval with probability 1 and can never return to the boxed area in Fig. 3.5, which may also be seen from its stationary distribution in Fig. 3.6. The sign of $[m] \gtrless 0$ depends on the initial state m_0, and on the realization of the driving field sequence in case the initial value is $m_0 \in [-m_2, m_2]$. This leads to the conclusion that the system is in a *ferromagnetic* phase.

Consider again the case of low temperature but with a strong driving field, as depicted in Fig. 3.1. As in the paramagnetic phase at high temperature, there is only one fixed point for each branch. Hence the trapping effect seen in the ferromagnetic phase cannot occur, even below the equilibrium critical temperature. The situation is best described as a *driven paramagnetic* phase. The corresponding stationary magnetization distribution is shown in Fig. 3.7. Note the possibility of type I intermittency around $m \approx 0$, to which we will come back to in the next section.

The most interesting case occurs when the field H_0 is such that $m_1 > m_2 = m_3$, which is possible at $K > 1$. It is easy to see that the branches then tangentially touch the diagonal at $m^\dagger = \pm m_2$, see Fig. 3.8. The corresponding distribution is depicted in Fig. 3.9. The fixed point equation for

[2] Taking a close look, you may notice that $P(m)$ is not *exactly* symmetric around $m = 0$. This is a numerical artifact due to the finite number of iterations and the limited resolution of the graph.

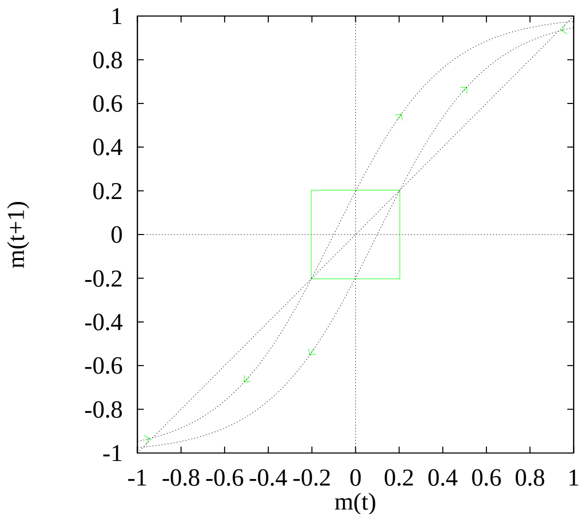

Figure 3.5: Same as Fig. 3.3, but for $K = 2.0$ and $\frac{H_0}{K} = 0.1$. Points initially inside the box marked in green are eventually mapped outside the box and can never return. Thus the system shows ferromagnetic behavior.

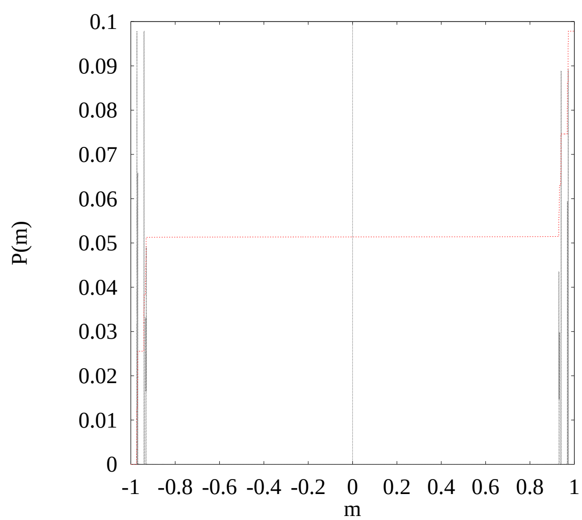

Figure 3.6: The stationary distribution of the map in Fig. 3.5. Again, the integrated distribution is shown in red.

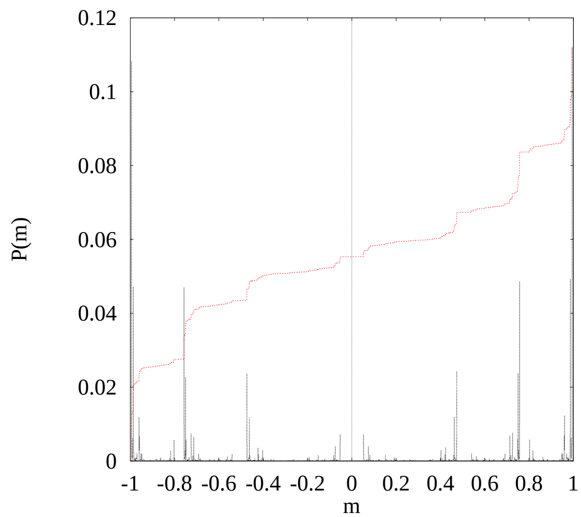

Figure 3.7: Stationary magnetization distribution for the map with $K = 2.0$ and $\frac{H_0}{K} = 0.5$ displayed in Fig. 3.1. Again, the scaled, integrated distribution is plotted in red. The system is in a driven paramagnetic phase.

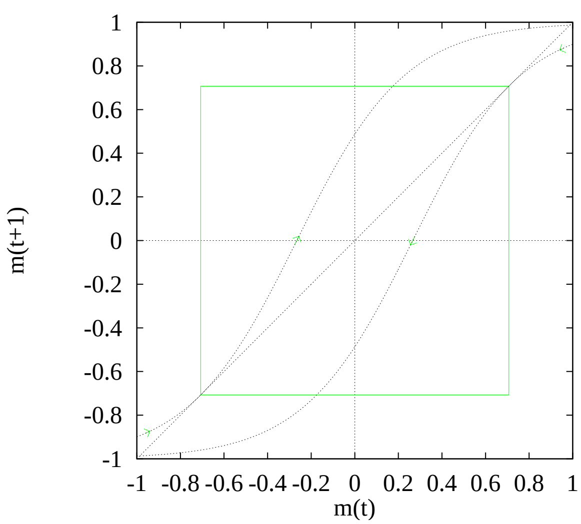

Figure 3.8: Same as Fig. 3.3, but for $K = 2.0$ and $\frac{H_0}{K} = 0.266$, close to the critical field. Points initially inside the green box are mapped outside eventually.

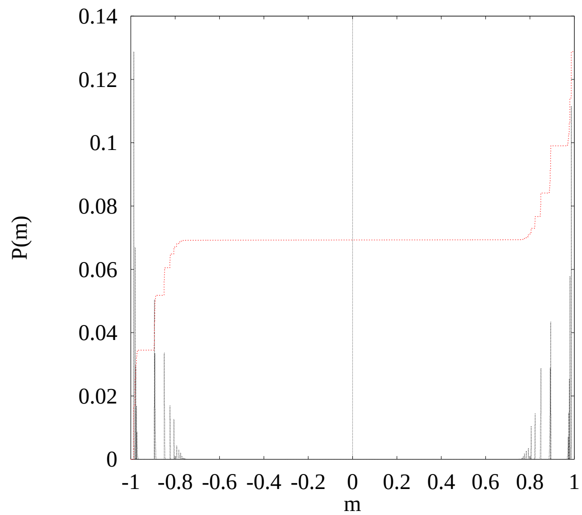

Figure 3.9: Magnetization distribution corresponding to the map of Fig. 3.8.

$m^\dagger$ leads to

$$Km^\dagger + H_c = \frac{1}{2}\ln\left(\frac{1+m^\dagger}{1-m^\dagger}\right) \tag{3.12}$$

$$\Rightarrow H_c = \frac{1}{2}\ln\left(\frac{1+m^\dagger}{1-m^\dagger}\right) - Km^\dagger \tag{3.13}$$

For a given $K > 1$, it is at $H_0 = H_c$ that a second, distinct fixed point appears. As long as $H_0 > H_c$, no trajectories can be trapped, as discussed above. But as soon as $H_0 \leq H_c$, the stationary magnetization $[m]$ is *bounded away from zero* by $|m^\dagger|$, for example $\sqrt{\frac{1}{2}}$ in Fig. 3.8. The RDIM is thus subject to a first order phase transition. The results for the critical field, Eq. (3.10) and (3.13), are shown in Fig. 3.10.

3.3 Dynamic freezing

The phase transition of the RDIM takes place due to dynamic freezing, which will be explained in this section. Fig. 3.11 displays the map at $K = 2$ for a driving field slightly above the critical one, $\frac{H_0}{K} = 0.3 \gtrsim \frac{H_c}{K}$. The green arrows indicate the movement of $m(t)$ through an "intermittent tunnel" which has

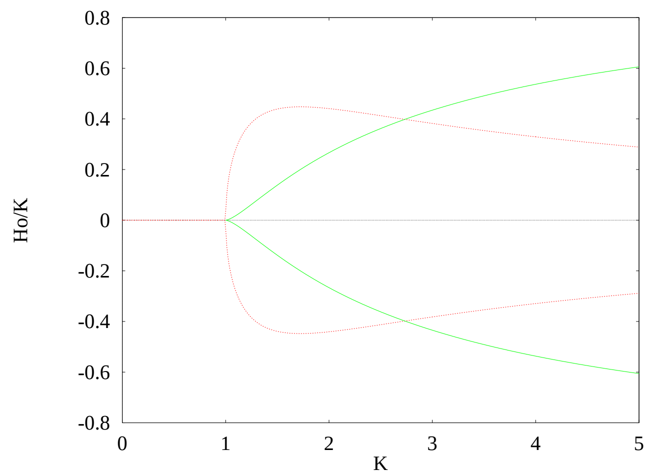

Figure 3.10: Phase diagram of the mean field RDIM. The red line corresponds to the critical field derived from an expansion of moments, Eq. (3.10). The green line is the transition obtained in the geometric discussion, Eq. (3.13).

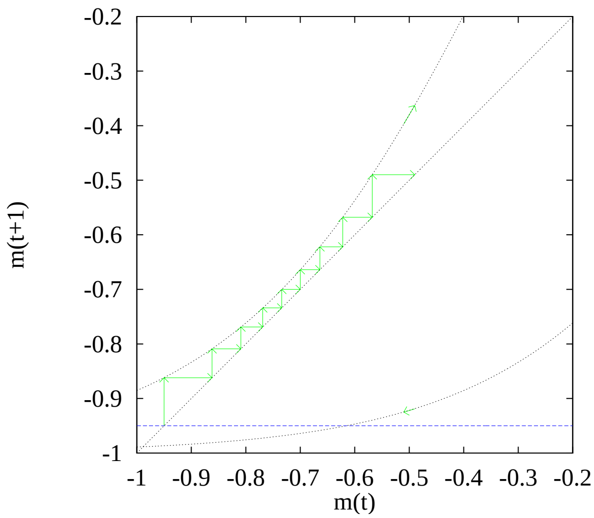

Figure 3.11: Intermittent mean field map at $K = 2$ and $\frac{H_0}{K} = 0.3$, slightly above the critical driving field. Starting at $m_0 = -0.95$, iteration along the upper branch f_+ is indicated by the series of green arrows. As long as $m(t) \lesssim -0.6$, taking a single step along f_- reinjects the trajectory into the region $m < -0.95$. This is indicated by the blue line.

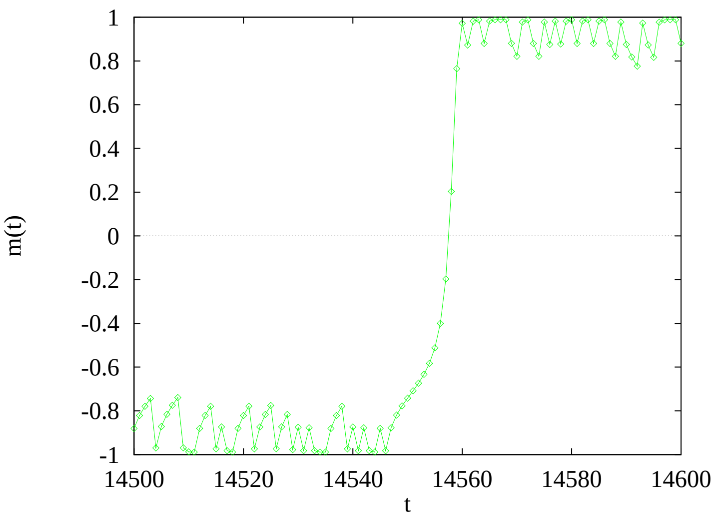

Figure 3.12: Part of a trajectory of the map in Fig. 3.11 is shown where escape from the region around m_3 occurs. The "laminar" regime shows a sawtooth dynamics. The intermittent burst in the middle of the graph is characterized by a monotonous increase of $m(t)$, after which the system settles again in a "laminar" regime.

to be passed in order to escape from the region around the negative fixed point m_3. Part of a trajectory is shown in Fig. 3.12 where this happens the first time. The "laminar" behavior of the magnetization is sawtooth-like, as can be seen in the left and right part of the trajectory. The monotonous increase in the middle of the graph is the intermittent burst.

Consider first what happens when iterating along the upper branch of the map only. As in the theory of chaotic maps (see [PoMa80]), $f_+(m) = \tanh(Km + H_0)$ is approximated to second order at $m^\dagger$, in the middle of the tunnel, for fields close to H_c:

$$m_{t+1} \approx m^\dagger + (m_t - m^\dagger) + \frac{H_0 - H_c}{K} + \frac{1}{2}\Big\{-2Km^\dagger(m_t - m^\dagger)^2 \\ -4m^\dagger(m_t - m^\dagger)\frac{H_0 - H_c}{K} - 2Km^\dagger\left(\frac{H_0 - H_c}{K}\right)^2\Big\} \quad (3.14)$$

Changing variables $x_t := m_t - m^\dagger$, small deviations of the driving field from

H_c lead to

$$x_{t+1} = x_t + \alpha x_t^2 + \epsilon, \tag{3.15}$$

where $\alpha := -Km^\dagger > 0$ and $\epsilon := \frac{H_0 - H_c}{K} > 0$. The difference equation may be approximated by the differential equation

$$\frac{dx}{dt} = \alpha x^2 + \epsilon, \tag{3.16}$$

from which the number of steps in the tunnel may be approximated by

$$n := t_{out} - t_{in} = \int_{x_{in}}^{x_{out}} \frac{dx}{\epsilon + \alpha x^2} = \frac{1}{\alpha\epsilon} \arctan\left(x\sqrt{\frac{\alpha}{\epsilon}} \right) \Big|_{x_{in}}^{x_{out}}. \tag{3.17}$$

Typically, one assumes that after exiting from the tunnel, $|x| > x_{out}$, a trajectory is reinjected into the tunnel at $|x| < x_{out}$ with probability $P(x) = P(-x)$. The expectation of the number of steps in the tunnel is

$$\langle n \rangle = \frac{1}{\alpha\epsilon} \arctan\left(x_{out}\sqrt{\frac{\alpha}{\epsilon}} \right). \tag{3.18}$$

The result for $x_{out}\sqrt{\frac{\alpha}{\epsilon}} \gg 1$ is

$$\langle n \rangle \sim \epsilon^{-\frac{1}{2}} = \left(\frac{H_0 - H_c}{K} \right)^{-\frac{1}{2}}. \tag{3.19}$$

This behavior is known as an inverse tangent bifurcation in literature[3].

But what happens to the RDIM in a parameter range where the above discussion is applicable? We need to iterate on average $\langle n \rangle = \left(\frac{H_0 - H_c}{K}\right)^{-\frac{1}{2}}$ steps along the upper branch, which happens with probability $p_{\langle n \rangle} = 2^{-\langle n \rangle}$. Each time the field is $-H_0$, the trajectory is moved back to the entrance of the tunnel, as indicated by the blue line in Fig. 3.11. Therefore, the escape rate for a population of $N(t)$ trajectories starting near m_3 is governed by

$$\dot{N}(t) = -const\ 2^{-\langle n \rangle}\ N(t), \tag{3.20}$$

yielding the mean escape time

$$\tau_{esc} = const\ 2^{\langle n \rangle} \sim 2^{(H_0 - H_c)^{-\frac{1}{2}}}. \tag{3.21}$$

Dynamic freezing occurs because τ_{esc} diverges exponentially as the driving field approaches the critical field value from above, $H_0 \mapsto H_c$.

[3]See, for example, the book by Schuster[Sc88]

3.4 The multifractal regime

Recall that the RDIM is an IFS (see Sec. 2.2), which suggests that the magnetization distribution will be a fractal in a certain parameter range. This is indeed the case.

As already mentioned, the values of $m(t)$ in the stationary state are limited to the interval $[-m_1, m_1]$. As is obvious from the top graph of Fig. 3.13, if $Km_1 - H_0 < 0$ there is a gap

$$\begin{aligned}\Delta = \tanh(-Km_1 + H_0) - \tanh(Km_1 - H_0) \\ = 2\tanh(H_0 - Km_1) > 0 \quad (3.22)\end{aligned}$$

of values around $m = 0$ that cannot be reached from either branch of the map. Therefore, the support of the invariant density is fractal with dimension $d_F < 1$ in the paramagnetic region up to the boundary line given by $Km_1 = H_0$ displayed in red in Fig. 3.14. Following the notation developed in [Ra93], the magnetization distribution is singular-continuous with fractal support (SC-F).

Taking a closer look at the map in the ferromagnetic region, displayed in the bottom graph of Fig. 3.13, there is another possibility for a gap to open. In the stationary state, the dynamics is confined to the interval $[m_1, -m_3]$[4], which implies

$$\Delta := \tanh(-Km_3 + H_0) - \tanh(Km_1 - H_0) > 0 \quad (3.23)$$

$$\Leftrightarrow \quad K(m_1 + m_3) < 2H_0. \quad (3.24)$$

The magnetization distribution in the ferromagnetic phase is also singular-continuous with fractal support in the region bounded by $K(m_1+m_3) = 2H_0$. In Fig. 3.14, its boundary is marked in blue.

Obviously, *something* happens in between these two regions. To this end, introduce the generalized dimensions of a set (as first reported in [HePr83]). For the limit set of the IFS represented by the mean field map, they are

$$d_q := \frac{1}{q-1} \lim_{\epsilon \mapsto 0} \frac{1}{\ln \epsilon} \ln \int d\mathcal{P}_s(m) \mathcal{P}_s(B_\epsilon(m))^{q-1} \quad (3.25)$$

where $q \geq 0$ and $B_\epsilon(m)$ is a ball of diameter ϵ around m. A numerically more tractable definition is given by Halsey *et al* [HaJe86], where balls of different

[4] Or $[-m_1, m_3]$, but we will look only at the positive interval.

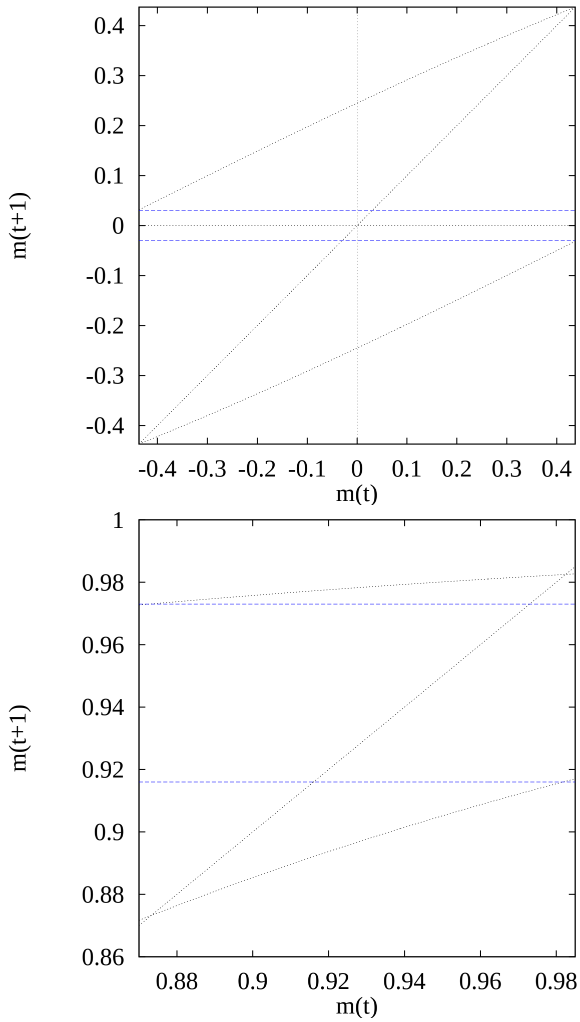

Figure 3.13: Top: Gap in the paramagnetic mean field map for $K = 0.5$ and $\frac{H_0}{K} = 0.5$. Values in the area demarked by the blue lines cannot be accessed. Bottom: The same in the ferromagnetic phase at $K = 2$ and $\frac{H_0}{K} = 2$.

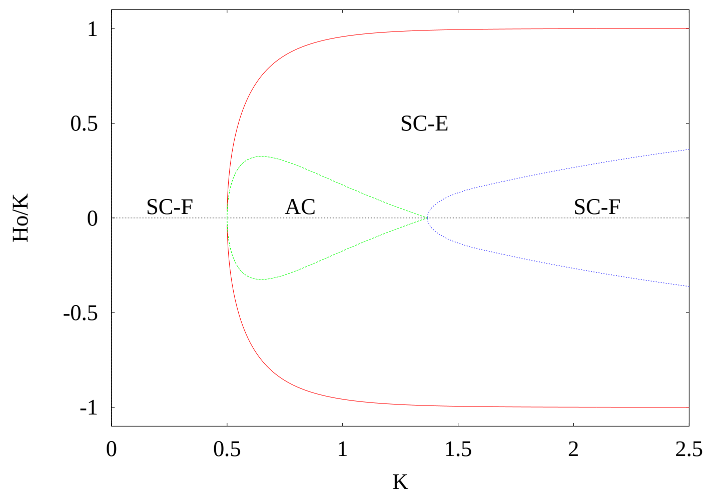

Figure 3.14: Classification of the RDIM's magnetization distributions following [Ra93].

diameters are used to cover a set[5]. They define a kind of partition function

$$\Gamma_N(q,\tau) := \sum_{i=1}^{N} \frac{p_i^q}{l_i^\tau} \tag{3.26}$$

where l_i is the length of the i-th interval needed to cover N disjoint sets. p_i is the probability associated with the i-th interval. Then there is a unique τ for which Γ is non-zero and finite in the limit $N \mapsto \infty$, which is used to define the generalized dimensions via

$$(q-1)d_q := \tau(q). \tag{3.27}$$

The Legendre transform of $-\tau(q)$ leads to the so-called multifractal spectrum

$$f(\alpha(q)) := q\frac{\partial\tau}{\partial q} - \tau(q) = q\alpha - \tau(q). \tag{3.28}$$

The minimum scaling index $\alpha_{min} \equiv d_\infty$ corresponds to the most concentrated

[5]This is a good thing to do as it leads to $d_f \equiv d_0 \equiv d_{Hausdorff}$. The latter is a dimension in a mathematically rigorous sense.

region of $\mathcal{P}_s$. Following [Ev87],

$$d_\infty = -\frac{\ln 2}{\ln f'_\pm}\Big|_{m_1}, \tag{3.29}$$

hence the border $d_\infty = 1$ is given by

$$K(1 - m_1^2) = \frac{1}{2}, \tag{3.30}$$

which is the green line in Fig. 3.14. Note that in the region marked AC (for absolutely continuous), all generalized dimensions are $d_q = 1$ and the magnetization distribution is square integrable in the usual sense (see [Ra93]). In the area marked SC-E (for singular-continuous with euclidean support), the support of the distributions is the complete interval $m \in [-1, +1]$. Here, only those generalized dimensions with $q > 0$ may be less than unity. This situation occurs in all three regions of the phase diagram.

3.5 A comment on the driving field

One may suspect that the properties of the RDIM discussed so far are due to the fact that we are looking at a binary driving field. Consider now a field uniformly distributed in the interval $I := [-H_{lim}, H_{lim}]$. The evolution of the RDIM is now given by choosing $H_0 \in I$ at each time step and following a mean field map

$$m(t+1) = \tanh(Km(t) + H_0). \tag{3.31}$$

Trajectories are generated by choosing from a continuum of maps in each time step, so to speak. The limiting maps for $H_0 = \pm H_{lim}$ are shown in green in Fig. 3.15. The critical maps for $H_0 = \pm H_c$ are displayed in red. Recall now the discussion of the dynamic freezing transition. Say a trajectory has run into the region $m \approx -1$. Then, as long as

$$H_{lim} > H_c = \frac{1}{2}\ln\left(\frac{1 - m^\dagger}{1 + m^\dagger}\right) + Km^\dagger, \tag{3.32}$$

there are maps allowing escape from this region. The probability to chose such a map is obviously

$$p_{esc} = \frac{1}{2H_{lim}}(H_{lim} - H_c) = \frac{1}{2}\left(1 - \frac{H_c}{H_{lim}}\right) < \frac{1}{2}. \tag{3.33}$$

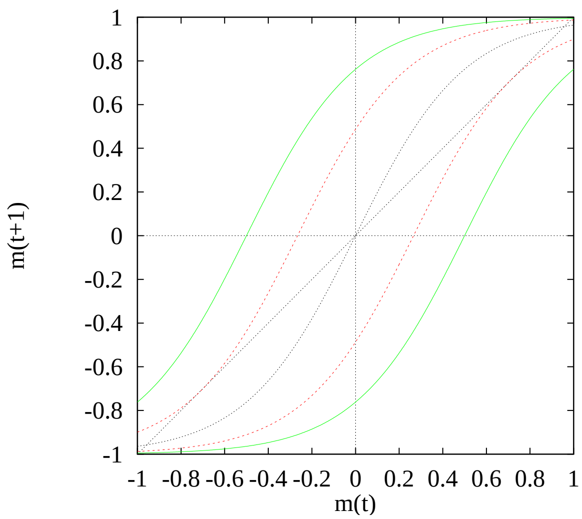

Figure 3.15: For a uniform distribution of the driving field, $H_0 \in [-H_{lim}, +H_{lim}]$, a continuum of maps is available which is bounded by the limiting maps shown in green. As long as the critical maps, displayed in red, are inside the continuum, the RDIM remains paramagnetic. The phase transition occurs at $H_{lim} = H_c$. The zero field map corresponding to the non-driven Ising model is shown in black.

From Eq. (3.19) for $H_0 = H_{lim}$ one deduces

$$\langle n \rangle > \left(\frac{H_{lim} - H_c}{K} \right)^{-\frac{1}{2}} \tag{3.34}$$

as maps closer to H_c than H_{lim} may be chosen. Thus, one may be sure to underestimate the escape time by

$$\tau_{esc} \sim \left(\frac{2H_{lim}}{H_{lim} - H_c} \right)^{(H_{lim}-H_c)^{-\frac{1}{2}}} . \tag{3.35}$$

Therefore, as before in the case of a binary-valued driving field, there is a freezing transition. The time averaged magnetization, which is the order parameter, remains zero until $H_{lim} \leq H_c$. Then, it again immediately jumps to a value $[m] \gtrless m^{\dagger}$. The arguments presented to describe the phase transition of the RDIM thus hold even for continuous driving field distributions, as long as there is a limiting field value H_{lim}.

This is in contrast to the results presented in [Ac98], who numerically solved the mean field dynamic equation of motion. There, it is claimed that the transition is continuous. This result may be due to the fact that the escape time (3.35) is extremely diverging. Hence, the order parameter must be calculated for very long times, otherwise it may indicate a phase transition where there is none.

This chapter has revealed some surprising properties of the RDIM in mean field approximation. The phase transition from para- to ferromagnetic behavior is first order, the order parameter jumps. The transition takes place due to dynamic freezing, which leads to a bifurcation of the stationary magnetization distribution. The latter is a multifractal for a wide parameter range. In both phases, there are regimes where the support of the magnetization distribution is a true fractal with $d_F < 1$. Finally, the restriction to a dichotomic driving field distribution is not so severe. The freezing transition also takes place, for example, for a uniform distribution in an interval. The critical ingredient is the existence of limiting maps, that is, the set of driving field strengths must be bounded. In the next chapter, the discussion will be extended to the one dimensional case.

Chapter 4

One Dimension

This chapter is devoted to the analysis of the RDIM in one dimension. The coarse grained Master Equation (2.20) here leads to maps for the local magnetization and two spin correlations, in a similar fashion as in the mean field case. Solutions for the translation invariant sectors are presented. Then, the phase transition at $T_c = 0$ is discussed. These results are formally similar to those of [Gl63] for a non-driven Ising model. Finally, the map of the translation invariant magnetization again leads to a distribution with fractal support.

4.1 Local magnetization and two spin correlations

The energy of the one dimensional Ising chain is given by

$$E = -J \sum_{i=1}^{N} s_i s_{i+1} + \mu_B B(t) \sum_{i=1}^{N} s_i, \tag{4.1}$$

where $s_{N+1} = s_1$ for periodic boundary conditions. The Glauber transition rate describing the Liouville operator is now

$$w(s_i) := w(\vec{\mu}_i|\vec{\mu}) = \frac{1}{2\alpha}\Big(1 - s_i \tanh\big(K(s_{i-1} + s_{i+1}) + H\big)\Big) \tag{4.2}$$

where $K = \beta J$ and $H = \beta \mu_B B$ are defined as before. For the local magnetization

$$m_i(t) = \langle s_i \rangle_t = \sum_{\vec{\mu}} s_i P(\vec{\mu}, t), \tag{4.3}$$

the time evolution may be calculated from (see [Gl63])

$$\dot{m}_i(t) = -2\langle s_i w(s_i) \rangle_t = \frac{1}{\alpha}\Big(- m_i(t) + \langle \tanh\big(K(s_{i-1} + s_{i+1}) + H\big)\rangle_t \Big). \tag{4.4}$$

Using again the coarse grained Master Equation and measuring time in units of τ_B, one obtains a map similar to the mean field one, namely

$$m_i(t+1) = \langle \tanh\big(K(s_{i-1} + s_{i+1}) + H\big)\rangle_t. \tag{4.5}$$

Defining the constants $\gamma = \tanh 2K$ and $h = \tanh H$, Eq. (4.5) may be transformed to the spin product representation

$$m_i(t+1) = \left\langle \frac{h}{2}\left(\frac{1-\gamma^2}{1-\gamma^2 h^2} + 1\right) + \frac{\gamma}{2}\left(\frac{1-h^2}{1-\gamma^2 h^2}\right)(s_{i-1} + s_{i+1}) + \frac{h}{2}\left(\frac{1-\gamma^2}{1-\gamma^2 h^2} - 1\right) s_{i-1}s_{i+1} \right\rangle_t . \tag{4.6}$$

In a more compact form,

$$m_i(t+1) = a + \frac{\widetilde{\gamma}}{2}(m_{i-1}(t) + m_{i+1}(t)) + d\langle s_{i-1}s_{i+1}\rangle_t \tag{4.7}$$

with

$$a := \frac{h}{2}\left(\frac{1-\gamma^2}{1-\gamma^2 h^2} + 1\right) \tag{4.8}$$

$$d := a - h \tag{4.9}$$

$$\widetilde{\gamma} = \gamma\left(\frac{1-h^2}{1-\gamma^2 h^2}\right). \tag{4.10}$$

Thus, for the driving field distribution (2.21), the dynamics of the one dimensional model are subject to the map

$$m_i(t+1) = \begin{cases} a + \widetilde{\gamma}\frac{m_{i-1}(t)+m_{i+1}(t)}{2} + d\langle s_{i-1}s_{i+1}\rangle_t \text{ with } p = \frac{1}{2} \\ -a + \widetilde{\gamma}\frac{m_{i-1}(t)+m_{i+1}(t)}{2} - d\langle s_{i-1}s_{i+1}\rangle_t \text{ with } p = \frac{1}{2}, \end{cases} \tag{4.11}$$

where a, d, and $\widetilde{\gamma}$ are evaluated at $h = \tanh H_0$. Again following [Gl63], one obtains for the two spin correlation $c_{i,j} = \langle s_i s_j \rangle_t$

$$\dot{c}_{i,j} = -2\langle s_i s_j \big(w(s_i) + w(s_j) \big) \rangle_t. \tag{4.12}$$

Now, choosing the time unit $\alpha = 2\tau_B$ leads to another map,

$$c_{i,j}(t+1) = \frac{1}{2}\langle s_j \tanh\big(K(s_{i-1}+s_{i+1})+H\big)+s_i\big(K(s_{j-1}+s_{j+1})+H\big)\rangle_t. \tag{4.13}$$

For $H = 0$, note that $a = d = 0$ and $\widetilde{\gamma} = \gamma$. As expected, the results due to [Gl63] are reproduced.

The last term of the local magnetization map (4.7) indicates that it is coupled to the two spin correlation $c_{i-1,i+1}(t)$. Similarly, transformation of Eq. (4.13) would show that the correlation map couples to a three spin correlation $c_{i,j,k}(t)$, and so forth. This means that one can get some results for the translation invariant sectors, but the others are unsolvable. Recall that the dynamic average of a spin function satisfies $[A(t+1)] = [A(t)]$, hence

$$[m_i] = \left[\frac{\widetilde{\gamma}}{2} \left(m_{i-1} + m_{i+1} \right) \right]. \tag{4.14}$$

Therefore, the translation invariant magnetization $m(t) = \frac{1}{N}\sum_i m_i(t)$ obeys

$$[m] = \widetilde{\gamma}[m] \tag{4.15}$$

as $[a] = [d] = 0$ due to the driving field symmetry and where $\widetilde{\gamma}$ is again evaluated for $h = \tanh H_0$, explicitly

$$\widetilde{\gamma} = \tanh(2K) \frac{1 - \tanh^2(H_0)}{1 - \tanh^2(H_0)\tanh^2(2K)}, \tag{4.16}$$

The translation invariant two spin correlation, $c_j(t) = \frac{1}{N}\sum_i c_{i,i+j}$, gives

$$[c_j] = \left[\frac{\widetilde{\gamma}}{2} (c_{j-1} + c_{j+1}) \right], \tag{4.17}$$

the solution of which is (again, refer to [Gl63])

$$[c_j] = \eta^{|j|} \text{ with } \eta = \frac{1 - \sqrt{1 - \widetilde{\gamma}^2}}{\widetilde{\gamma}}. \tag{4.18}$$

Note that even though the recursion relations Eqs. (4.14) and (4.17) are formally equivalent, they do not have the same solution. The solution given for $[c_j]$ rest upon the fact that $c_0 \equiv 1$, whereas generally $m_0 \neq 1$ (see [Gl63]).

4.2 The phase transition at $T_c = 0$

Similar to the non-driven case, the magnetization of the one dimensional RDIM vanishes except for $\widetilde{\gamma} = 1$, which requires $K \mapsto \infty$ (corresponding to $T \mapsto 0$). A ferromagnetic phase may only exist at $T_c = 0$. From Eq. (4.16) it is easy to see that $\lim_{K\mapsto\infty} \widetilde{\gamma} = 1$ if H_0 is fixed. But if additionally $H_0 \mapsto \infty$, one may run into trouble[1].

To make this more precise, consider the correlation length ξ, which is related to η by

$$\eta^{|j|} \sim e^{-\frac{|j|}{\xi}} \Rightarrow \xi = -\frac{1}{\ln \eta}. \tag{4.19}$$

It is straightforward to rewrite $\widetilde{\gamma}$ in terms of exponentials in K and κ,

$$\widetilde{\gamma} = \frac{(1 - e^{-4K})(2 + e^{-4K(1-\kappa)} + e^{-4K(1+\kappa)})}{8(1 + e^{-8K} + e^{-4K(1-\kappa)} + e^{-4K(1+\kappa)})} \tag{4.20}$$

with $\kappa := \frac{H_0}{2K}$. Expansion of $\widetilde{\gamma}$ near $T_c = 0$ leads to

$$\widetilde{\gamma} \approx \begin{cases} 1 - e^{-4K(1-\kappa)} & \text{for } \kappa < 1, \\ e^{-4K(\kappa-1)} & \text{for } \kappa > 1. \end{cases} \tag{4.21}$$

From Eq. (4.15), $[m] = 0$ due to $\widetilde{\gamma} = 0$ for $\kappa > 1$. Thus, in addition to the paramagnetic behavior for $T > 0$, the RDIM remains in a paramagnetic phase in the $T = 0$ limit provided that the driving field is strong enough. This corresponds to the driven paramagnetic phase discussed in the mean field approximation. For weaker fields, $\kappa < \kappa_c = 1$, there is a symmetry-breaking ferromagnetic phase.

Inserting Eq. (4.21) in Eq. (4.19) one finds that the correlation length is in leading order

$$\xi \sim \begin{cases} e^{2K(1-\kappa)} & \text{for } \kappa < 1, \\ \frac{1}{4K(\kappa-1)} & \text{for } \kappa > 1. \end{cases} \tag{4.22}$$

The relaxation time corresponding to the decay of the order parameter, the translation invariant magnetization, reads

$$\frac{1}{\tau_{sys}} = 1 - \widetilde{\gamma} \sim \begin{cases} \xi^{-2} & \text{for } \kappa < 1, \\ 1 & \text{for } \kappa > 1. \end{cases} \tag{4.23}$$

[1] Recall that $H_0 = \beta\mu_B B_0 = K\mu_B B_0/J$. Thus the limit $H_0 \mapsto \infty$ occurs naturally in the low temperature limit provided B_0 is fixed.

In a strong field situation, $\kappa > 1$, all spins on the chain follow the external driving field. Furthermore, Eq. (4.23) tells us that for temperatures near T_c, the spins are almost always parallel to the field. Conversely, if $\kappa < 1$, the system's relaxation time is proportional to the square of the correlation length, that is, τ_{sys} diverges with critical dynamic exponent $z = 2$. Yet, from Eq. (4.22), the divergence of ξ *decreases* continuously with κ. A physical explanation reconciling these results is presented in the next section.

4.3 Kink dynamics

In order to understand why the critical dynamic exponent remains $z = 2$ even though the divergence of the correlation length decreases with $\kappa < 1$, one needs to analyze the behavior of domain walls.

First, take a look what happens to a domain barrier at $H_0 = T = 0$. From Eq. (4.2), the interface between two domains of oppositely oriented spins, a *kink*, moves left or right with $p = \frac{1}{2}$, which may be interpreted as a random walk. If the typical domain length is ξ, two such kinks meet via diffusive motion in the characteristic time $\tau \sim \xi^2$, which is the reason why $z = 2$. Once there is only one spin left between two kinks they annihilate with probability $p = 1$ in the next time step and the two domains merge. An example of this kink dynamics for a closed chain of two thousand spins tracked for five hundred time steps is depicted in Fig. 4.1. The situation is similar in the neighborhood of $T_c = 0$.

Switching on the external driving field (with $\kappa < 1$) causes domains with spins parallel to the field start to grow. The kinks at the end of such a cluster move outwards one step during each time step where the field remains favorable. If the field switches into the unfavorable direction, the cluster shrinks again. This "breathing" behavior is displayed in Fig. 4.2. From the transition rate Eq. (4.2) it is clear that for $\kappa = 1$ nucleation *inside* a cluster becomes possible with probability $p = \frac{1}{2}$. Consider now, for example, that the external field takes on the value $+H_0$ $(\tau + n)$-times in 2τ iteration steps. Due to the driving field distribution, this occurs with a probability given by the Bernoulli distribution, $p_{2\tau}(n) = \binom{2\tau}{\tau+n}2^{-2\tau}$. At $T = 0$, a domain of down spins of length L_0 will shrink to $L_0 - 2n$ and will thus be eliminated if $L_0 \leq 2n$. Due to the fact that $\langle n^2 \rangle = \frac{\tau}{2}$, the random walk of the field is expected to deviate from $\langle n \rangle = 0$ by $\sqrt{\frac{t}{2}}$ at time step t. Therefore, one expects either *all*

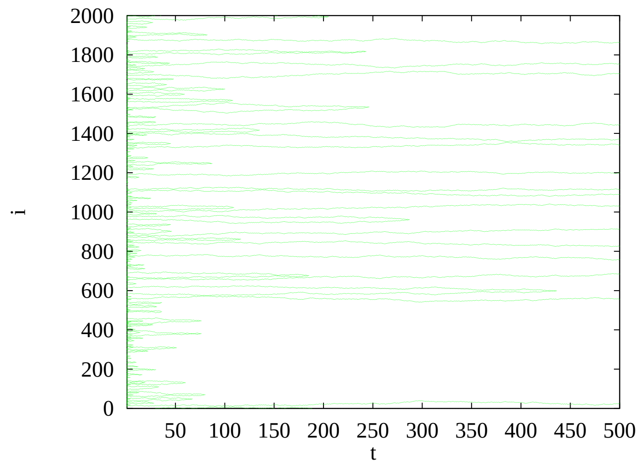

Figure 4.1: Zero temperature kink dynamics for $\kappa = 0$, the non-driven case. The graph shows the location i of kinks vs. time t, which may be interpreted as a random walk.

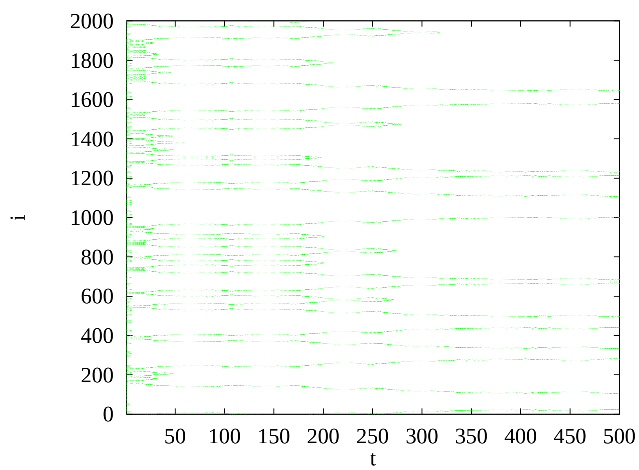

Figure 4.2: Zero temperature kink dynamics for $0 < \kappa < 1$. The clusters "breathe" in accordance with a favorable or unfavorable driving field. Note the rapid depletion of small domains in comparison with the non-driven case, Fig. 4.1.

up domains or *all* down domains of size $L_0 \leq \sqrt{\frac{\tau}{2}}$ to vanish. Note that small domains and the kinks associated with them will be eliminated rapidly, as can be seen by comparing Figs. 4.2 to 4.1. However, once only a few large clusters remain, the kinks again perform a random walk. Here, it is due to the driving field dynamics that we recover $z = 2$.

4.4 The fractals are back...

In the previous chapter it was shown that the stationary probability distribution induced by the mean field map displays multifractal behavior. In the present case, a part of these results may be recovered.

From the local magnetization map (4.11) the map for the translation invariant magnetization is

$$m(t+1) = \begin{cases} \widetilde{\gamma} m(t) + a + dc_2(t) =: f_+(m(t)) \text{ with } p = \frac{1}{2} \\ \widetilde{\gamma} m(t) - a - dc_2(t) =: f_-(m(t)) \text{ with } p = \frac{1}{2}. \end{cases} \tag{4.24}$$

In order to decouple $m(t)$ from the two spin correlation $c_2(t)$, one may approximate the latter with its stationary value, $c_2(t) \approx [c_2] = \eta^2$. Hence, in the stationary state both branches $f_\pm$ are linear and there is one fixed point each, $m_\pm := \pm \frac{a+d\eta^2}{1-\widetilde{\gamma}}$. An example map and the corresponding stationary distribution $P(m)$ for $K = 0.2$ and $H_0 = 0.4$ is shown in Fig. 4.3. A gap opens up if

$$\Delta := f_+(m_-) - f_-(m_+) = \frac{2(a + d\eta^2)(1 - 2\widetilde{\gamma})}{1 - \widetilde{\gamma}} > 0 \tag{4.25}$$

As a, d, and $1 - \widetilde{\gamma}$ are positive and $c_2(t) \in [0, 1]$ for ferromagnetic coupling $J > 0$, the condition for a gap is $\widetilde{\gamma} < \frac{1}{2}$. But note that the border between fractal and non-fractal support given by $\widetilde{\gamma} = \frac{1}{2}$ is actually *independent* of η^2, and hence $c_2(t)$. Therefore, in this regime the map Eq. (4.24) always induces a fractal support. The boundary $H_F(K)$ may easily be calculated from Eq. (4.10),

$$h_F \equiv \tanh H_F = \pm \sqrt{\frac{1 - 2\gamma}{\gamma^2 - 2\gamma}} \tag{4.26}$$

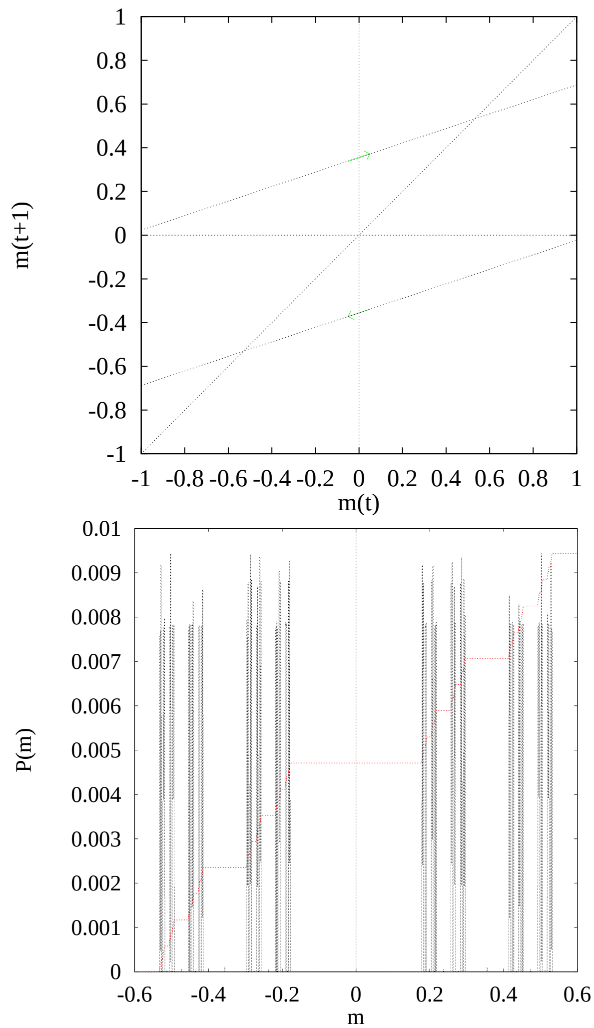

Figure 4.3: Top: Truncated one dimensional magnetization map with $\Delta > 0$. Parameters are $K = 0.2$ and $H_0 = 0.4$. Bottom: The corresponding stationary magnetization distribution. Strictly speaking, the distribution should be constant on its support. The fluctuations seen here are due to the finite bin size.

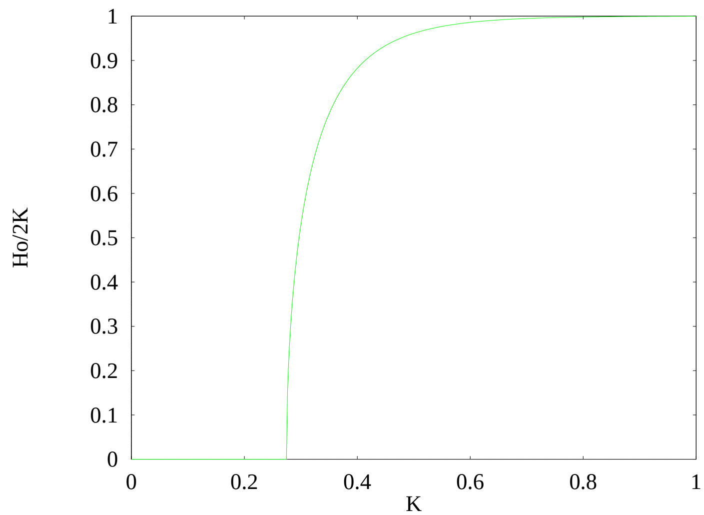

Figure 4.4: Boundary between regimes with fractal and non-fractal support of the magnetization distribution in the one dimensional case given by $\widetilde{\gamma} = \frac{1}{2}$. Unless $H_0 = 0$, the support is always fractal, $d_F < 1$, for $K < \frac{1}{4} \ln 3$.

which leads to

$$H_F = \frac{1}{2} \ln \left(\frac{\gamma^2 - 4\gamma + 1 + 2\sqrt{5\gamma^2 - 2\gamma - 2\gamma^3}}{1 - \gamma^2} \right). \tag{4.27}$$

In the stationary state, the magnetization distribution support is a strictly self-similar Cantor set. Its fractal dimension is

$$d_0 \equiv d_F = \frac{\ln 2}{\ln \left(2(a + d\eta^2)\widetilde{\gamma} \right) - \ln(1 - \widetilde{\gamma}).} \tag{4.28}$$

This result is displayed in Fig. 4.4. Unless $H_0 = 0$, the support is always fractal for $K < \frac{1}{4} \ln 3 \approx 0.275$.

We close here the discussion of the one dimensional RDIM. As in the mean field approximation, the coarse grained Master Equation leads to stochastic maps, of which the translation invariant sector may be solved analytically. The phase transition occurs at $T_c = 0$, similar to the non-driven case. A truly ferromagnetic phase requires that the driving field is not too strong, $\kappa < 1$. Again, the map of the translation invariant magnetization may lead to a fractal support of the magnetization distribution. The next chapter is concerned with the last purely physical model discussed in this thesis, the two dimensional Ising model.

Chapter 5

Two Dimensions

The two dimensional Ising model has been the subject of myriads of publications, yet no solution has been found for non-zero external magnetic fields. Therefore, all the results presented in this chapter are derived from numerical simulations, namely a Monte Carlo approach. As usual, the spins are arranged on a square lattice and interact with their four nearest neighbors. Generally speaking, the problem with such a simulation is that in addition to the thermal average, a dynamic average is required. To approximate these, as large a set as possible of trajectories has to be tracked. This requires a vast amount of computing power.

In the first section of this chapter, the Monte Carlo algorithm that allows for a parallel simulation of several RDIMs on the neurocomputer SYNAPSE-1/N110[1] is described. Next, a rough approximation of the phase diagram is presented. The chapter concludes with a discussion of the RDIM´s behavior in the para- and ferromagnetic phases, again focusing on the possibly multifractal character of the stationary magnetization distribution.

5.1 SYNAPSE visiting Monte Carlo

The name of the machine indicates what it originally was designed for: The fast solution of typical problems encountered when simulating artificial neural networks. Basically, this means fast matrix multiplications. In order to make efficient use of its computational power, we need a matrix Monte Carlo

[1]Pál Ruján and J.H. wish to express their gratitude to U. Ramacher at ZFE Siemens AG for kindly providing to us this machine for extensive simulations.

algorithm[2]. Such an algorithm may easily be designed for the parallel simulation of a population of similar models. This alleviates the problem of many long simulation runs mentioned above.

Consider an $L \times L$ square lattice of spins $s^k_{m,n} \in \{-1, 1\}$ where k denotes the number of the system and $m, n = 0, 1, \ldots, L-1$ specify the lattice coordinates. Ignoring for the moment the choice of boundary conditions, the nearest neighbors of a spin located at (m, n) are $\{(m, n \pm 1), (m \pm 1, n)\}$. Renumbering the spins s_i with $i = mL + n$ we find the set of neighbors is $\mathcal{N}(i) := \{i \pm 1, i \pm L\}$. Now, setting $i \mapsto i + L^2$ for $i < 0$ and $i \mapsto i - L^2$ for $i \geq L^2$ enforces helical boundary conditions. In this way, one lattice may be viewed as an L^2-dimensional vector $(s_0, s_1, \ldots, s_{L^2-1})$, and k systems can be represented as an $L^2 \times k$ matrix[3].

In two dimensions, the energy of one spin is

$$E_i = K \sum_{j \in \mathcal{N}(i)} s_i s_j + H s_i \tag{5.1}$$

where $K = \beta J$ and $H = \beta \mu_B B$ as before. Thus the Glauber dynamic rule is

$$w(s_i) := w(\vec{\mu}_i | \vec{\mu}) = \frac{1}{2} \left(1 - s_i \tanh \left(K \sum_{j \in \mathcal{N}(i)} s_j + H \right) \right), \tag{5.2}$$

and time is measured in units of $\alpha = \tau_B$ again. The well-known (local) Monte Carlo scheme to simulate an Ising system follows:

1. Start with $i = 0$.

2. Choose a random number $z \in [0, 1]$ from a uniform distribution.

3. If $z < \frac{1}{2} \left(1 - s_i \tanh \left(K \sum_{j \in \mathcal{N}(i)} s_j + H \right) \right)$, update the spin $s_i \mapsto -s_i$.

4. Repeat until all L^2 spins have been updated.

[2]SYNAPSE-1 is a coprocessor linked to a Sun workstation via S-BUS. It consists of a systolic array of eight neural signal processors MA16. The interface used to drive it is a set of C++ library functions implementing matrix operations.

[3]The systolic array of the neurocomputer always operates on fields of size 64×8, so k and L should be chosen accordingly.

This is usually called a Monte Carlo step (MCS)[4]. Recall that $H(t)$ is constant for intervals of length τ_B. Consequently, the value $\pm H_0$ of the driving field should remain fixed for a complete MCS, that is, the time unit is again set to τ_B. We need to adapt this scheme to the matrix representation described above.

The neurocomputer provides a parallel random number generator, therefore all the updates necessary for one MCS for all systems could be done in one step. Furthermore, matrices may be piped through function lookup tables at no extra computational cost. It makes sense to transform the above flip condition to

$$s_i \mapsto \begin{cases} -s_i & \text{if } \sum_{j\in\mathcal{N}(i)} s_i s_j < \frac{1}{2K}\ln\left(\frac{0.5-z'}{0.5+z'}\right) - s_i\frac{H(t)}{K}, \\ s_i & \text{else,} \end{cases} \tag{5.3}$$

where z' is drawn from a uniform distribution on $[-\frac{1}{2},\frac{1}{2}]$. In this way, the terms in Eq. (5.3) may be generated in four ELementary OPerationS (ELOPS). The RHS of the flip condition requires the generation of a random number matrix piped through the lookup table $z' \mapsto \frac{1}{2K}\ln\left(\frac{0.5-z'}{0.5+z'}\right)$ and one weighted matrix addition. The LHS requires a convolution type matrix multiplication and an elementwise matrix product. Two further ELOPs are necessary to construct and evaluate a flip indicator matrix.

There is a small technical problem, namely, a simultaneous update leads to non-physical metastable states[5]. To avoid this, the spins in each lattice are split into a checkerboard of black and white sites. One ends up with *two* matrices encoding the k RDIMs, each containing the neighbor sites of the other. For simplicity, each spin vector is augmented with a copy of its first and last row at the end, respectively beginning. Note, though, if L is odd, the spins of the first and last row have neighbors of their own color. If L is even, this is true for the first and last columns. For technical reasons we choose L odd. These sites need to be treated separately, which is computationally not problematic as they are not in bulk.

After proper initialization of the matrices representing the black and white spins, we are ready to specify the algorithm we need. One MCS is taken by:

[4] Often, the spins on the lattice are not run through sequentially. Rather, one repeats the procedure $N \sim L^2$ times, choosing at random the site i for each update

[5] A non-driven system, for example, runs into an antiferromagnetic configuration even though the coupling $J > 0$ is ferromagnetic.

1. Randomly choosing the direction of the driving field for this MCS, $H(t) = \pm H_0$.
2. Calculation of the terms in Eq. (5.3) (4 ELOPS).
3. Generation of a flip indicator matrix for the black sites (1 ELOPS).
4. Updating the black sites (1 ELOP).
5. Repeating Steps 2. to 4. for the white sites (6 ELOPS).
6. Fixing the blocks corresponding to the first and last row.

Some more operations are required to calculate the mean magnetization of each lattice.

The result presented in the following sections are calculated from two variants of this scheme. For the large lattices of size 415×415, we simulate eight systems. Each of these is subject to the same external driving field. The spins of each lattice are initialized to $s_i = +1$ with probability p and $s_i = -1$ with $1 - p$ where $p = 0, 0.2, 0.4, 0.5, 0.6, 0.8,$ and 1.0 In addition, there is one lattice with all spins up in the upper half and all spins down in the lower half. The phase diagram is computed from parallel simulation of 64 smaller lattices (size 143 or 63×63). Here, each system has its own driving field trajectory. All spins are initialized to $s_i = +1$ with probability $p = \frac{1}{2}$. For completeness, the snapshots shown are taken from a run of a *single* RDIM of size 128×128. Note that this is the only case where the boundary conditions are periodic, *not* helical. Again, all spins are initialized to $s_i = +1$ with probability $p = \frac{1}{2}$.

One further note before the discussion of the simulation results. The temperature K in this chapter is normalized with the critical temperature of the non-driven two dimensional Ising model, $K_c = \frac{J}{k_B T} = \frac{1}{2}\ln(1+\sqrt{2}) \approx 0.44$. In this way, $K = 1$ corresponds to the critical temperature at $H_0 = 0$.

5.2 Dynamics and phase diagram for two dimensions

To start off this section, the $T = 0$ dynamics of the two dimensional RDIM is analyzed. Next, the behavior of an equilibrium state at $H \equiv -H_0$ is considered when switching the field to the unfavorable direction $H = +H_0$

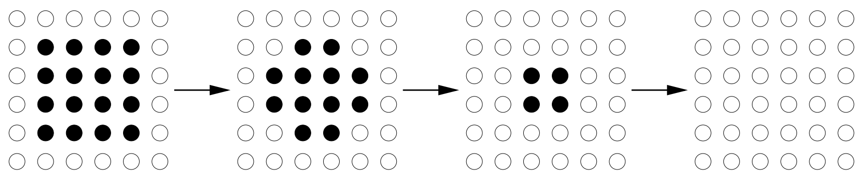

Figure 5.1: Annihilation of a 4×4 cluster at $T = 0$ and $0 < \kappa' < 1$ in three steps. Only the corner spins follow the external field, which favors the white sites.

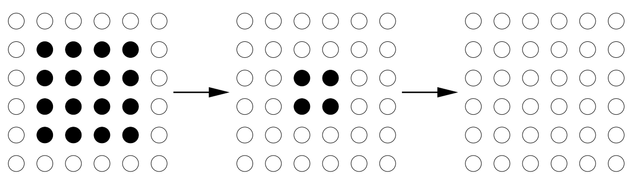

Figure 5.2: Annihilation of a 4×4 cluster at $T = 0$ and $1 < \kappa' < 2$ in two steps. Here, only the inner spins do not follow the external field.

and how this relates to the RDIM. Finally, a rough approximation to the phase diagram is presented.

In analogy to the discussion of kink dynamics for the one dimensional model, one may ask what happens to a (square) cluster of $2N \times 2N$ parallel spins at $T = 0$. According to Eq. (5.2), transition rates are $0, \frac{1}{2}$, or 1 in this limit. Recalling that K is measured in units of K_c, define $\kappa' := \frac{H_0}{2K} = \kappa K_c$. Assume now that the external field is antiparallel to the cluster's spins. It is easy to see that for a weak field $0 < \kappa' < 1$, the corner spins flip with probability $p = 1$. All others remain antiparallel to the field. Therefore, the cluster disappears if the external field remains in the unfavorable direction for $2N - 1$ consecutive steps. This is shown in Fig. 5.1. Next, in the medium field range $1 < \kappa' < 2$, edge spins additionally flip with $p = 1$. Only at inner sites do they remain antiparallel to the external field. Hence, a cluster is destroyed in N steps, as displayed in Fig. 5.2. Moving on to strong fields $\kappa' > 2$, there exists again a driven paramagnetic phase. All spins will flip parallel to the driving field with $p = 1$. In the cases $\kappa' = 0$, $\kappa' = 1$, and $\kappa' = 2$ the corner, edge, and inner spins flip with $p = \frac{1}{2}$, respectively. For example, at $\kappa' = 1$, the edges of a cluster may roughen. At $\kappa' = 2$, nucleation flips may take place *inside* a cluster. This type of behavior also occurs at $T > 0$.

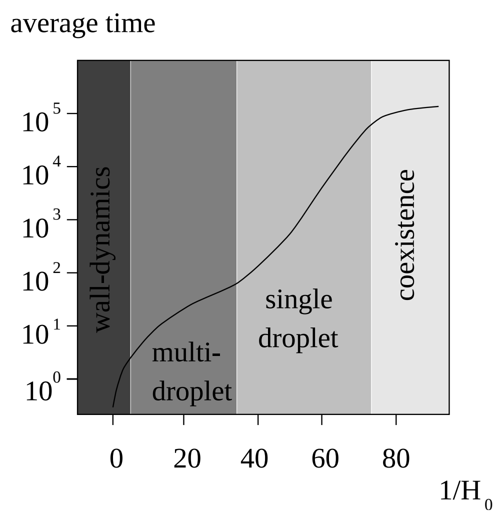

Figure 5.3: Average lifetime of a metastable state as a function of inverse field strength.

The next question to address is what happens to an equilibrium state of the non-driven model at $H(t) \equiv -H_0$ when switching the field to the unfavorable direction, $H(t) = +H_0$. Obviously, the system will relax from the now metastable state to the new equilibrium state. The lifetime of the metastable state depends on the strength of the external field. This has been discussed in detail in the ferromagnetic phase both numerically, via Monte Carlo simulation, and theoretically using droplet theory [RiTo94]. There, four distinct regimes were identified according to their main decay mechanism, displayed schematically in Fig. 5.3. Numerically, the average lifetime is calculated by approximating the average first passage time (FPT) of the system's mean magnetization $m := \sum_i s_i$ from the equilibrium value[6] at $-H_0$ to $m = +0.7$. As an example, this relaxation at $K = 1.25$ and $\frac{H_0}{K} = 0.08$ is shown on the top of Fig. 5.4. The average magnetization and its standard deviation is evaluated at each time step from an ensemble of 64 systems of size 143×143. All spins were initialized to $s_i = -1$. For comparison purposes, the result of a mean field iteration started at $m = -1$ with $K = 1.2$ and $\frac{H_0}{K} = 0.057$ is shown on the bottom.

[6]Or simply starting from $m = -1$.

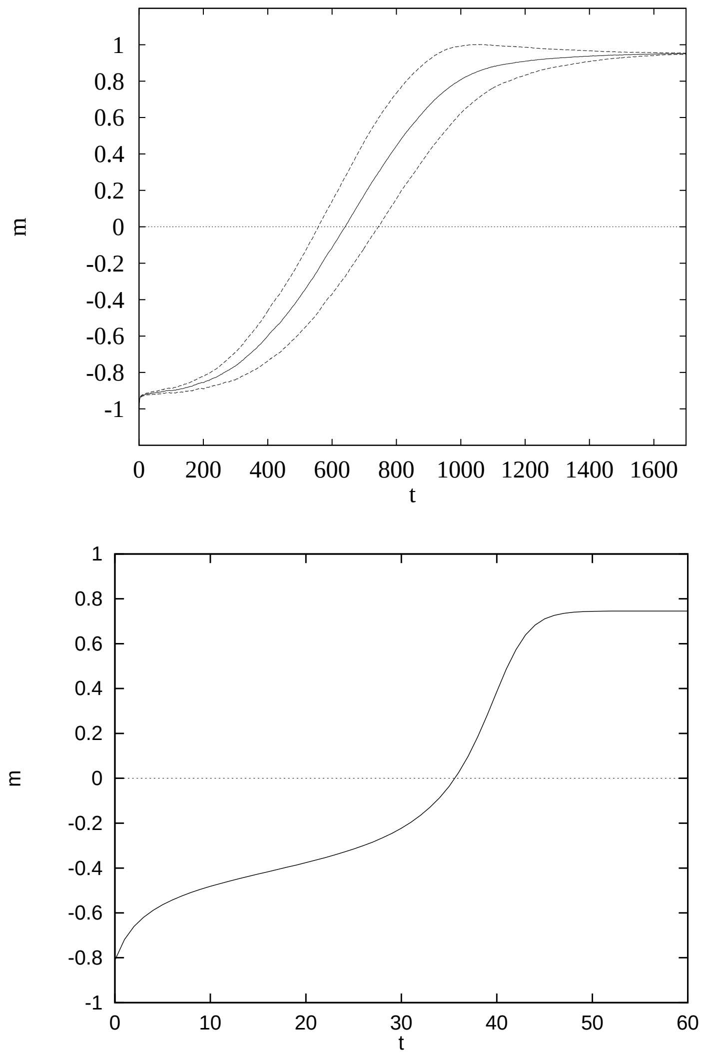

Figure 5.4: Top: Monte Carlo simulation showing the relaxation of the two dimensional model at $K = 1.25$ in a constant unfavorable field $\frac{H_0}{K} = 0.08$. The solid line is the average magnetization at time t from 64 systems of linear dimension $L = 143$, the dotted lines demark a 1-σ range. Bottom: Mean field iteration at $K = 1.2$ and $\frac{H_0}{K} = 0.057$.

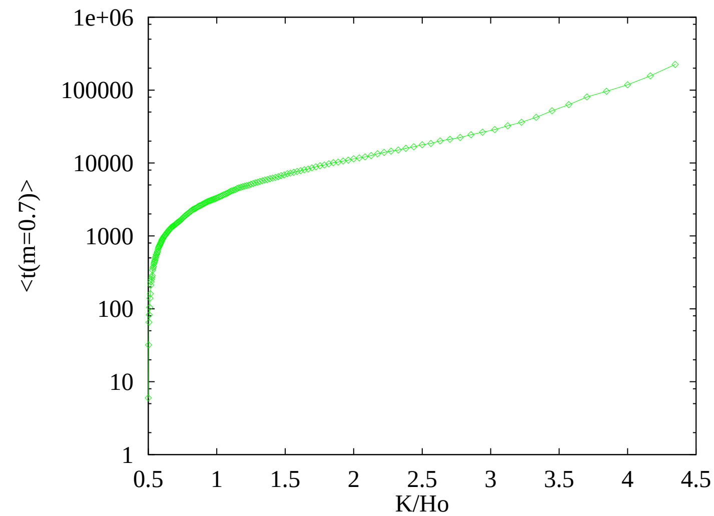

Figure 5.5: Average first passage time of the RDIM from $m = -1$ to $m = 0.7$ at $K = 1.25$ as a function of inverse field strength $\frac{K}{H_0}$ from Monte Carlo simulation of 64 systems of linear size $L = 143$.

The mean FPT $\langle t(m = 0.7)\rangle$ for the RDIM is shown in Fig. 5.5. Again, the number of MCSs required to reach $m = 0.7$ when starting at $m = -1$ is averaged from an ensemble of 64 systems of size L=143 at $K = 1.25$, slightly below the critical temperature of the non-driven model. For strong fields $\kappa' > 2$, the phase is driven paramagnetic. Due to the driving field distribution, $\langle t(m = 0.7)\rangle = \mathcal{O}(1)$ because the probability of the field *not* taking on the value $+H_0$ in the time interval $[0, t]$ is exponentially distributed, $p(t) = \lambda e^{-\lambda t}$ with $\lambda = \frac{1}{2}$. Keeping in mind that the field's random walk is expected to deviate from its expectation $\langle n\rangle = 0$ by $\sqrt{\frac{t}{2}}$ at time t, it is clear that the increase of the FPT with decreasing field is much larger than in the non-driven case with *constant* unfavorable field.

Finally, the top graph of Fig. 5.6 displays the phase diagram of the two dimensional RDIM. It was calculated numerically from a simulation of an ensemble of 64 systems of size $L = 63$. A driving field range from $H_0 = 0$ to $H_0 = 5$ was covered with step size $\Delta H = 0.5$. In turn, for each H_0, temperatures from $T = 1.5T_c$ to $T = 0.1T_c$ were evaluated with step size $\Delta T = 0.01T_c$. For each set of parameters (H_0, T) a simulation was run

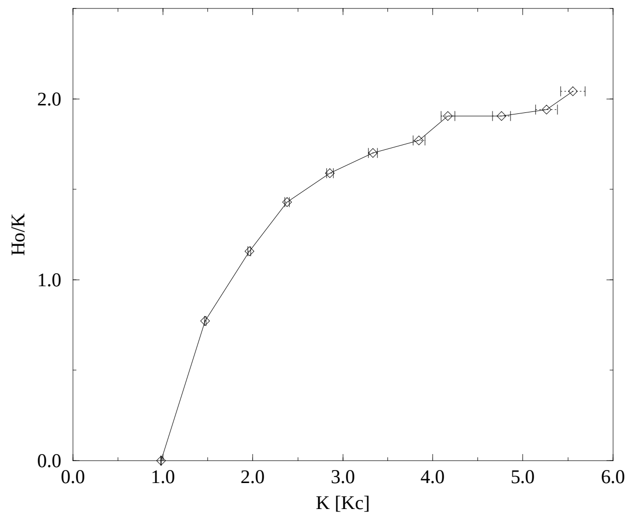

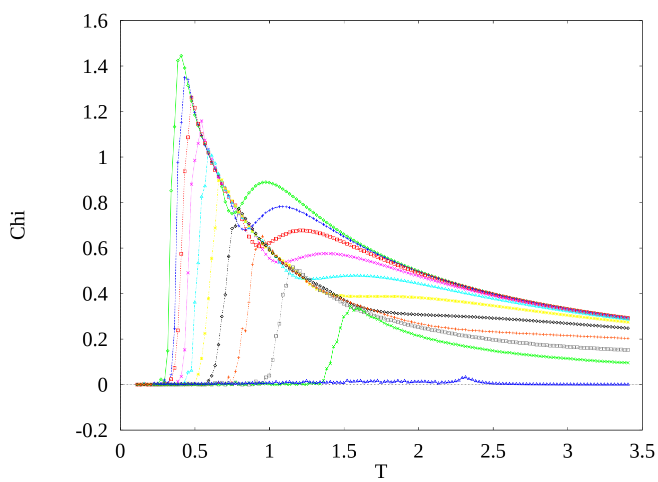

Figure 5.6: Top: Phase diagram of the two dimensional RDIM from a Monte Carlo simulation of 64 systems of size 63×63. The phase boundary should remain below $\frac{H_0}{K} = 2\kappa' = 4$ in the limit $K \mapsto \infty$. Bottom: Average magnetic susceptibilities χ for driving fields $H_0 = 0 \ldots 5$.

for eleven thousand MCS[7], tracking the first and second moment of each system's magnetization. One may numerically evaluate the susceptibilities $\chi_i(T, H_0) = \langle m_i^2 \rangle - \langle m_i \rangle^2$ for $i = 1, 2, \ldots, 64$, as well as the ensemble average $\chi(T, H_0)$, which is shown in the bottom graph of Fig. 5.6. The phase transition from para- to ferromagnetic behavior is now identified from the maxima of $\chi(T, H_0)$ at a given field strength H_0 with respect to T. As expected, the phase is paramagnetic for $K < 1$. For $K \geq 1$, there exists a critical field separating a ferromagnetic from a driven paramagnetic phase, similar to that of the mean field model. The phase boundary near $K = 1$ does not correspond to the first order transition seen in the mean field model. Rather, a second order transition seems likely, in qualitative agreement with further results of [Ac98]. There, a numerical study of the two dimensional Ising model with the driving field uniformly distributed in the interval $[-H_0, +H_0]$ also indicates a second order transition. Recall, though, the discussion of this type of field distribution for the mean field model in chapter 3.5. Due to the extremely long metastable lifetimes (Fig. 5.5) for weak driving fields, we cannot conclusively assess the order of the transition. Note also that in the low temperature limit, $K \mapsto \infty$, the phase boundary should approach $\kappa' = 2$ (corresponding to $\frac{H_0}{K} = 4$).

5.3 The para- and ferromagnetic phases

The RDIM shows paramagnetic behavior provided $H_0 > H_c$, where $H_c = 0$ for high temperature $K < 1$. In this phase, the system´s relaxation towards the stationary state is usually fast, as may be seen from Fig. 5.4. Similar to the kink dynamics discussed for the one dimensional model, the dynamics is determined by nucleation and annihilation, as well as radial growth and shrinking of droplet-like clusters. As the driving field approaches H_c, critical slowing down sets in due to effects similar to the type-I intermittency discussed in the mean field case (see chapter 3.3).

From the discussion of the mean field model, one expects to see an indication of fractality in the stationary magnetization distribution. Indeed, thermal fluctuations and finite size effects cannot completely erase this behavior, as shown in Fig. 5.7. The top graph displays $P(m)$ obtained from a numerical simulation at $K = 0.4$ and $\frac{H_0}{K} = 0.5$. Eight lattices of linear size $L = 415$ with different initial conditions were tracked for more than 2×10^5

[7] The first one thousand MCS are not taken into account.

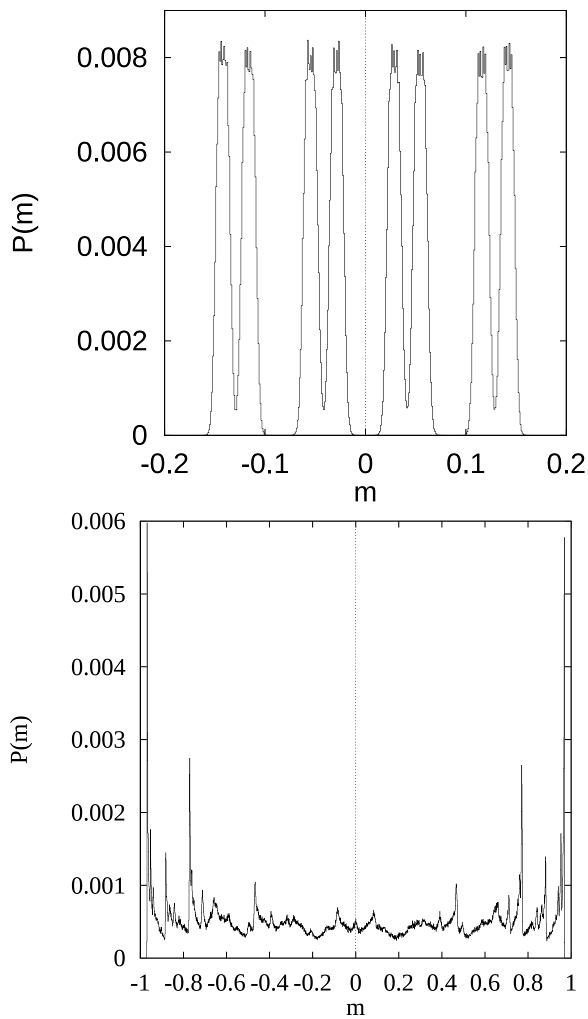

Figure 5.7: Top: Magnetization distribution of the two dimensional RDIM from eight systems of linear dimension $L = 415$ with different initial conditions. Parameters are $K = 0.4$, $\frac{H_0}{K} = 0.5$, and $\tau_B = 1$. The simulation ran for more than 2×10^5 MCS. Note the similarity to Fig. 3.3 in chapter 3, where the distribution of the mean field model is shown in the paramagnetic phase. Bottom: The same distribution for $K = 1.0$ and $\frac{H_0}{K} = 1.0$. Here, note the similarity to the driven paramagnetic case in the mean field model, Fig. 3.7.

MCS. Clearly, the distribution has a structure similar to the Cantor set of the mean field case, see Fig. 3.3. On the bottom, the stationary distribution at $K = 1$ and $\frac{H_0}{K} = 1$ from a corresponding simulation run is depicted. Note here the similarity to the driven paramagnetic distribution shown in Fig. 3.7. The sharp peaks in both distributions arise from droplets that are large enough to survive even long series of unfavorable field draws.

For $K \geq 1$ and $H_0 < H_c$, the RDIM is in the ferromagnetic phase. Recall that in mean field approximation the spontaneous magnetization distribution remained multifractal for a wide range of temperature and subcritical driving fields, Figs. 3.13 and 3.14. As shown in Fig. 5.8, this feature is retained in two dimensions. At the top, for $K = 2$ and $\frac{H_0}{K} = 1$ one finds a structure similar to that seen in Fig. 3.5, the mean field distribution in the ferromagnetic case. The bottom graph for $K = 1.33$ and $\frac{H_0}{K} = 0.75$ resembles the critical mean field distribution displayed in Fig. 3.8. In both cases there are well separated peaks which are smoothed out by the thermal fluctuations not present in the mean field model.

Finally, to indicate the complexity of the two dimensional model in the ferromagnetic phase, Fig. 5.9 shows a time series of the average magnetization of the RDIM. Only one model of linear dimension $L = 128$ with periodic boundary conditions is tracked at $K = 2$, $\frac{H_0}{K} = 1$, and $\tau_B = 1$. Note the intermittent bursts at times $t \approx 1000$, near $t \approx 4000$, and so on. Snapshots of the system of the stretches marked Series $1 \ldots 3$ are displayed on the following pages. We see both multidroplet (series 1 and 3) and domain-wall (series 2) type dynamics. Note also the droplet within droplet structures, for example at $t = 2900$ and $t = 16210$.

Clearly, there are indications that the two dimensional RDIM inherits some of the features of the mean field approximation and the one dimensional model. Parameters may be tuned to obtain magnetization distributions whose fine structure is smoothed out by thermal fluctuations. Yet, their similarity to mean field results is obvious. The $T = 0$ dynamics resembles the kink dynamics discussed in the one dimensional case. Yet, the phase transition does not correspond to the first order one seen in the mean field theory, a second order transition is more likely. As the computational effort required to achieve these results is already immense, the Monte Carlo study presented leaves open many interesting aspects of the model. For instance, the rough phase diagram should be computed in more detail with respect to

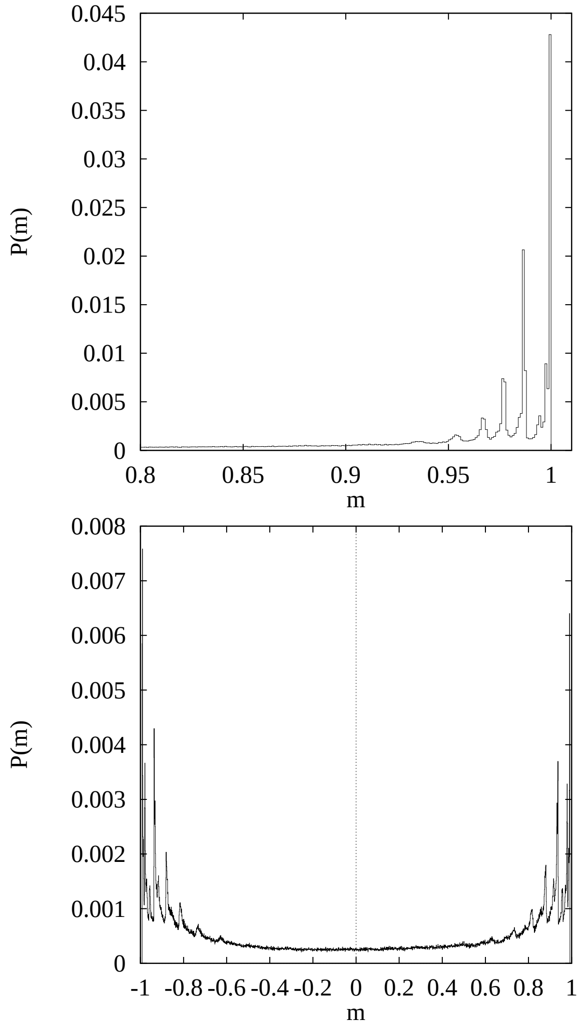

Figure 5.8: Magnetization distribution of the two dimensional RDIM in the ferromagnetic phase. As in Fig. 5.7, the linear dimension is $L = 415$ and $\tau_B = 1$. Top: $K = 2.0$ and $\frac{H_0}{K} = 1$, the simulation run covers more than 2×10^5 MCSs. Only the region from $m = 0.8$ to $m = 1.0$ is shown, the distribution is, of course, symmetric. It resembles that of the mean field model shown in Fig. 3.5. Bottom: $K = 1.33$ and $\frac{H_0}{K} = 0.75$, the simulation covers 1.5×10^5 MCSs. Compare to the critical mean field distribution in Fig. 3.8.

system size and the length of simulation runs, and analyzed regarding finite size scaling. Also, the dynamics of droplets or domain walls might prove to be an interesting topic. In the final chapter, the RDIM will be discussed from a more application oriented point of view: It may be reinterpreted as a very primitive model of spiking neural tissue – leading to a novel view of cortical noise.

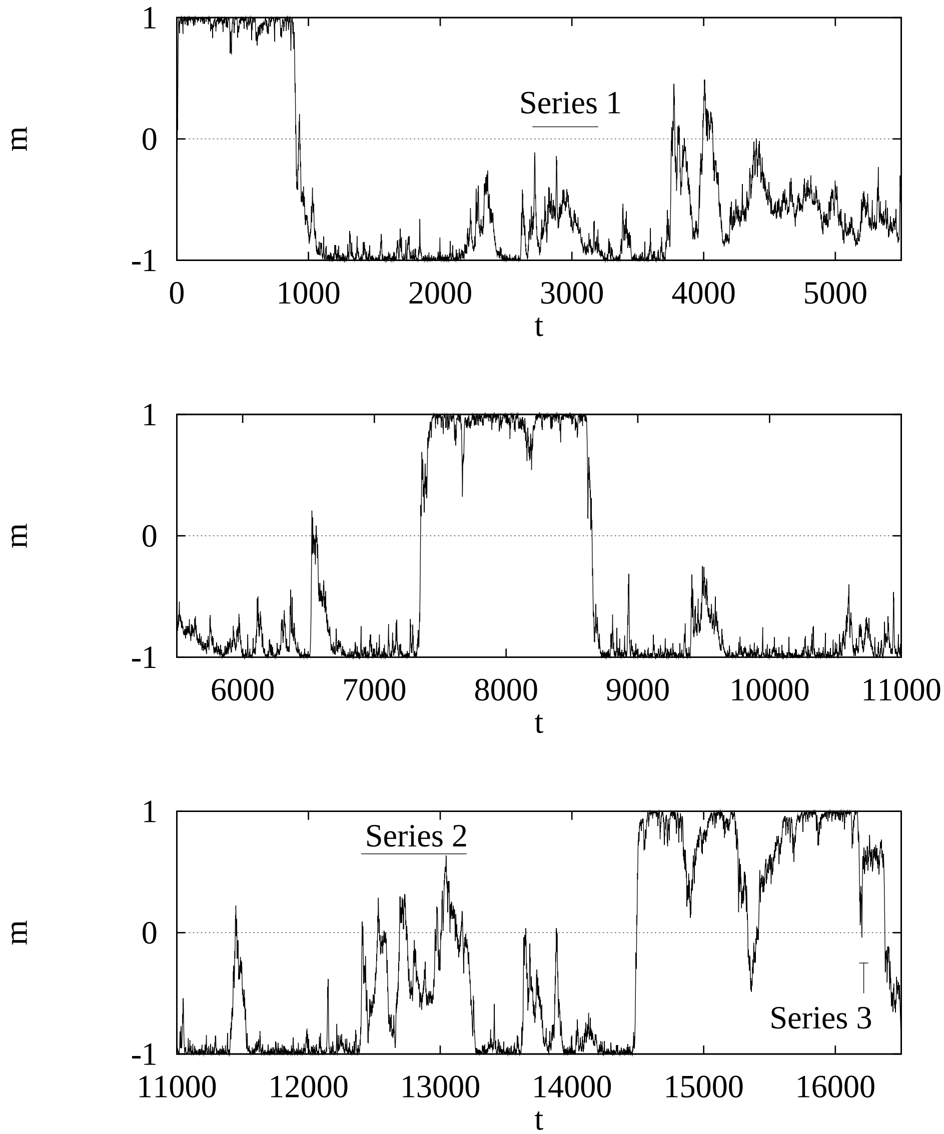

Figure 5.9: Time series of the mean magnetization of the two dimensional RDIM in the ferromagnetic phase. Parameters are $K = 2$, $\frac{H_0}{K} = 1$, $\tau_B = 1$, and the linear dimension is 128. Here, only one model with periodic boundary conditions was simulated. Snapshots of the system are shown for series 1, 2, and 3 on the next pages.

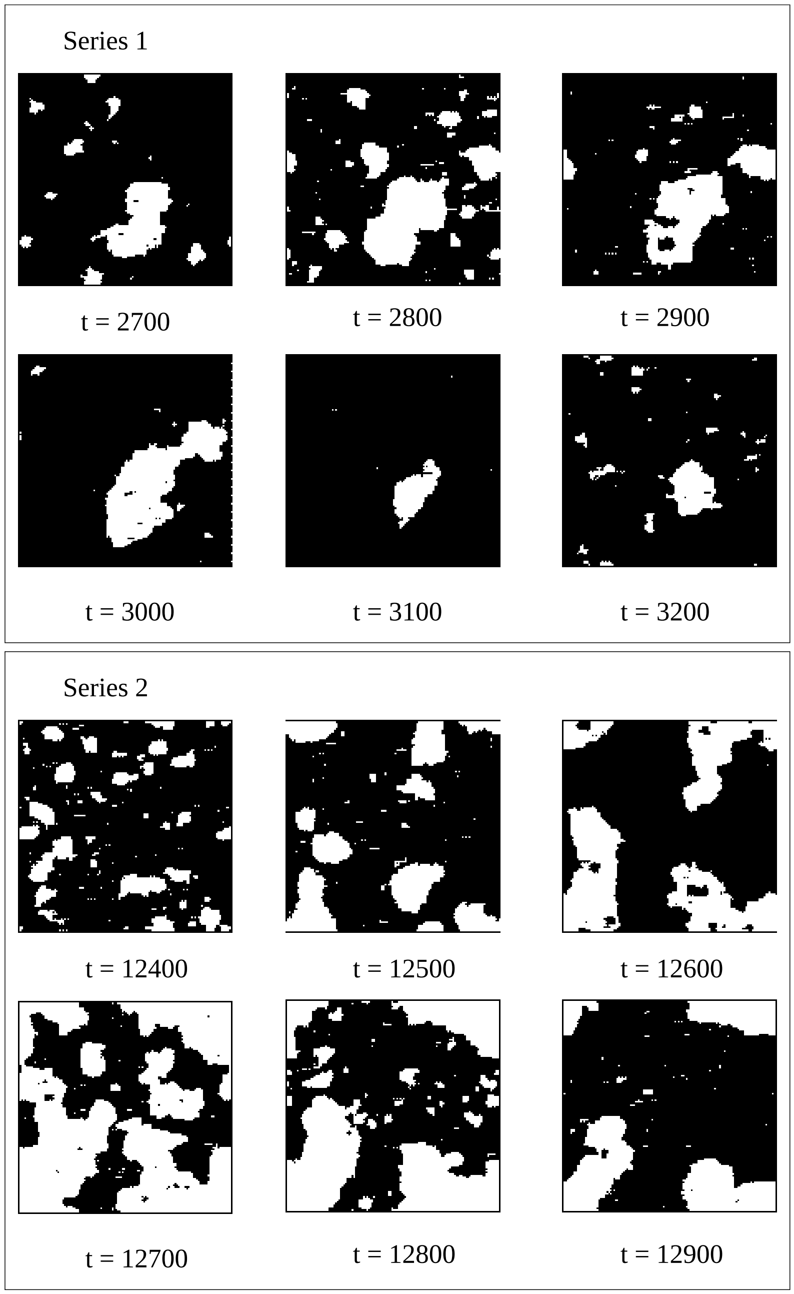
Series 1
t = 2700
t = 2800
t = 2900
t = 3000
t = 3100
t = 3200
Series 2
t = 12400
t = 12500
t = 12600
t = 12700
t = 12800
t = 12900

Series 2, continued

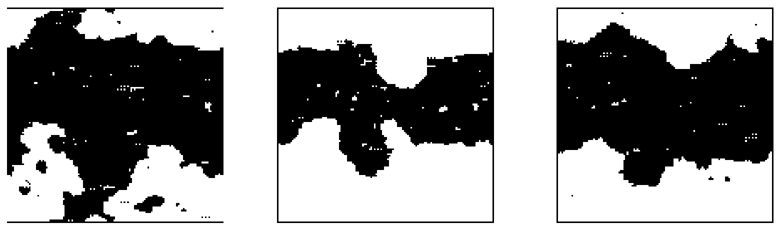

t = 13000 t = 13100 t = 13200

Series 3

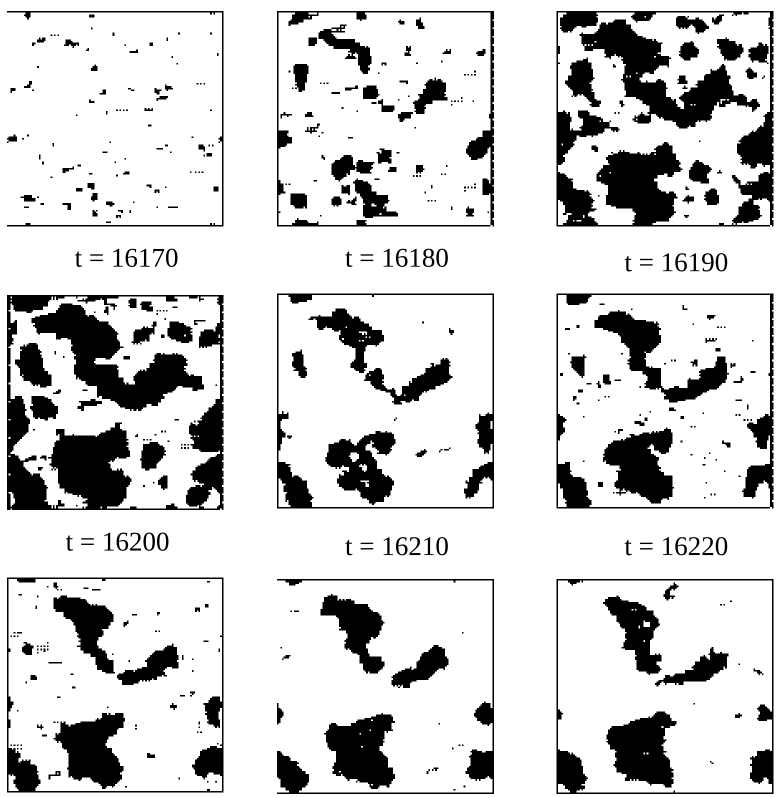

t = 16230 t = 16240 t = 16250

Chapter 6

On cortical noise

It is a well-known fact in neurobiology that communication between nerve cells (neurons) is based mainly on electrical impulses called spikes. A spiking neuron may thus be viewed as a simple input-output unit, gathering signals from and passing its own signal, or activity, to other nerve cells. The complexity of information processing in neural tissue, for instance the human brain, arises due to the sheer number of such units *and* their complex connectivity pattern[1]. To give an impression, the visual system from eye to cortex is schematically depicted in Fig. 6.1 (taken from [Ch89]). Incoming photons are detected by photoreceptors in the retina. The latter is an input device, so to speak, which transforms visual stimuli to spikes. These signals are passed on from ganglion cells, the last layer of cells in the retina, to the lateral geniculate nucleus (LGN) along the optic nerve. The LGN serves as a kind of traffic controller, feeding signals to different areas in the visual cortex.

From a neurobiological point of view, this chapter is rather abstract, so the reader is referred to the literature for an introduction to the field[2] . The following sections focus on how an Ising-type model may be interpreted as a very primitive model of neural tissue – and the role of the RDIM in this context. If one accepts the neural analogy, the consequences are the multifractal magnetization distributions, dynamic freezing, and the para- to ferromagnetic phase transition appearing in the physical model. These properties need to be interpreted in terms of information processing in nerve tissue – which leads far beyond this work. Yet, state of the art technology may be em-

[1]For example, the human cortex consists of around 10^{11} neurons, each of which is connected on average to one to ten thousand other neurons.

[2]A good kerman book is [Re90].

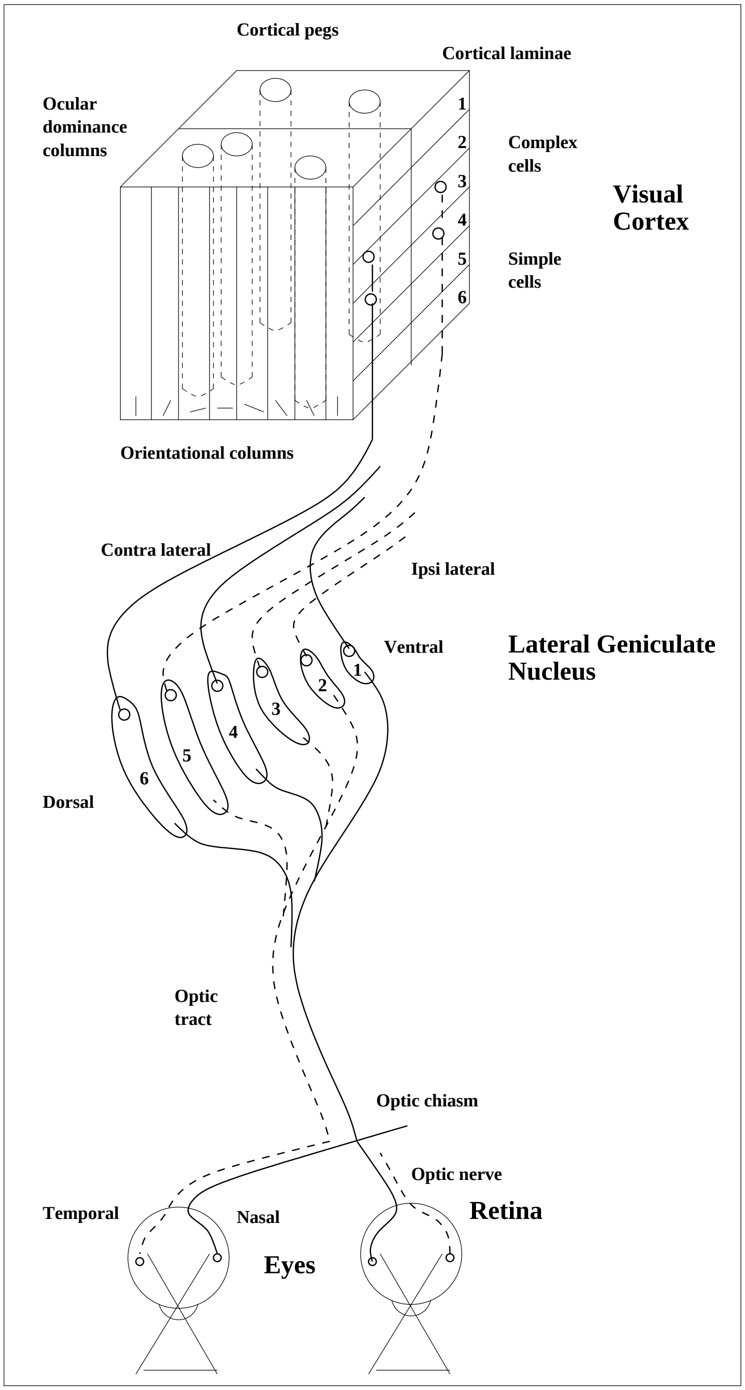

Figure 6.1: Primate visual system

ployed to examine experimentally if remnants of RDIM effects appear in such tissue. Similar to the experimental possibilities ultrathin ferromagnetic films present for the "physical" model, neurobiological experiments are waiting to be done.

6.1 The neurobiological interpretation of the RDIM

The complexity of the electrophysiological details of the process of spike generation and propagation in a *single* neuron is enormous. Neural communication based on chemical agents called neurotransmitters obscures the situation even more, to the point that it is currently absolutely hopeless to specify and handle a complete model of nerve tissue. A compromise between the level of detail of single cells versus their number has to be made. As the RDIM is a statistical mechanics model of externally driven coupled spins, the level of physiological detail will obviously be very low. Yet, due to the fact that neural communication may be viewed as digitized through the transmission of spikes, we may gain some insight about the behavior of neural assemblies driven by external stimuli.

Consider first the non-driven model. The system is intended to mimic a patch of neural tissue, or cell assembly. Each spin is interpreted as a neuron that may take on the states "spike", $s_i = +1$, or "no spike", $s_i = -1$ during each time step. As before, time is discretized in intervals τ_B. This is, of course, the first simplification we make – disregarding completely the chemical processes in the cells. In the mean field, one, or two dimensional model, each neuron-spin is connected to all others, its left and right neighbors, or its four nearest neighbors, respectively. In contrast to biological neural networks, these connections are all of the same strength J, and as the model is ferromagnetic, $J > 0$, there is no inhibitory mechanism. Both assumptions are typically not valid in real nerve tissue – the next simplification. The external driving field H_0 represents spikes arriving from *outside* the cell assembly. The strength of the field could be interpreted either with respect to the typical number of spikes arriving during the time unit τ_B, or with the impact of an input spike on the assembly. Finally, there is the notion of temperature T, an interpretation of which remains an open question at this point.

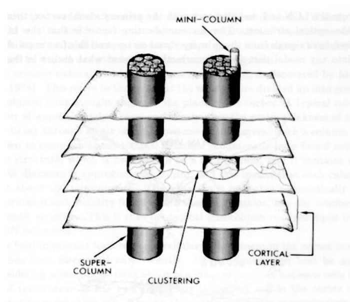

Figure 6.2: Structure of the primary visual cortex. Neurons are grouped in minicolumns perpendicular to the general six layer arrangement. Minicolumns are in turn grouped in supercolumns. Long-range connections between supercolumns lead to the formation of clusters.

Clearly, when subject to a stimulus constant in time, the system will evolve towards an equilibrium state – of which there is no indication in neurobiology. The interesting case occurs for time-dependent stimuli. The simple driving field dynamics of the RDIM may serve as a first approximation of sensory input[3]. Note that this field is homogeneous across all model neurons, hence one should consider assemblies of cells with a common receptive field. This situation is present, for example, in the primate visual cortex, where neurons are grouped in columns perpendicular to the general six layer structure (see Fig. 6.2, also taken from [Ch89]). The cells comprising these cortical pegs have such a common receptive field. Closer to the input side, photo receptors in the retina project onto neighboring ganglion cells, the first spiking neurons in the visual pathway. Thus, stimulating the eye with a large enough spot of light turned on and off at random again corresponds to a homogeneous external driving field.

[3]Which is not so unrealistic. Consider, for example, what must happen in the retina, and later on in the visual cortex, when you rapidly blink your eyes.

The results discussed in the previous chapters for the "physical" RDIM are mostly related to the mean magnetization. In the neural picture, this is equivalent to the *average* output signal of the neurons. Hence, the RDIM magnetization must be viewed as a *population code*, where $\frac{m(t)+1}{2}$ is the fraction of this population firing a spike at time t. Thus, the RDIM naturally leads to a nonequilibrium stationary code distribution. There is consent among neurobiologists that such populations play a major part in the neural information game, even though there are indications that the exact timing of individual spikes should not be ignored.

6.2 Asymmetric driving field distribution

Recall that the driving field distribution is symmetric, see Eq. (2.21). Thus, incoming spikes, corresponding to $+H_0$, appear with probability $p_+ = \frac{1}{2}$ in each time step. Alternately, the number of spikes n arriving in a given time interval $[0, \tau]$ follows a Poisson distribution, $p_n = \frac{\lambda^n}{n!} e^{-\lambda\tau}$ with $\lambda = \frac{1}{2} \equiv p_+$. This type of distribution is believed to approximate the spiking behavior in neural tissue, though not necessarily with $\lambda = \frac{1}{2}$. To control the frequency of external spikes one can tune λ by adjusting p_+ in the asymmetric field distribution

$$\rho(B) = p_+ \delta(B - B_0) + (1 - p_+)\delta(B + B_0). \tag{6.1}$$

From the results presented for the mean field RDIM in Chapter 3 one may deduce that this modification of the driving field distribution will have no major impact. The phase transition due to dynamic freezing does not depend on p_+ – except that two maps are required, $p_+ > 0$. Similarly, if a magnetization gap occurs, the associated distribution will again have a fractal support. The boundaries of the SC-F regions in Fig. 3.14 remain the same. This is generally not true for the SC-E and AC regions as the multifractal spectrum varies with p_+.

Four code distributions of the mean field map at $K = 1.0$ and $p_+ = 0.4$ are shown in Figs. 6.3 and 6.4 for different field strengths. This parameter range corresponds to driven paramagnetic behavior, even though the average magnetization is $m < 0$. Obviously, the probability for an inactive cell assembly, $m \approx -1$, is enhanced due to the asymmetric field. Yet, the structure of the distributions remains – it is *not* continuous and the codes may live on a fractal support. Note that these distributions are calculated in the same

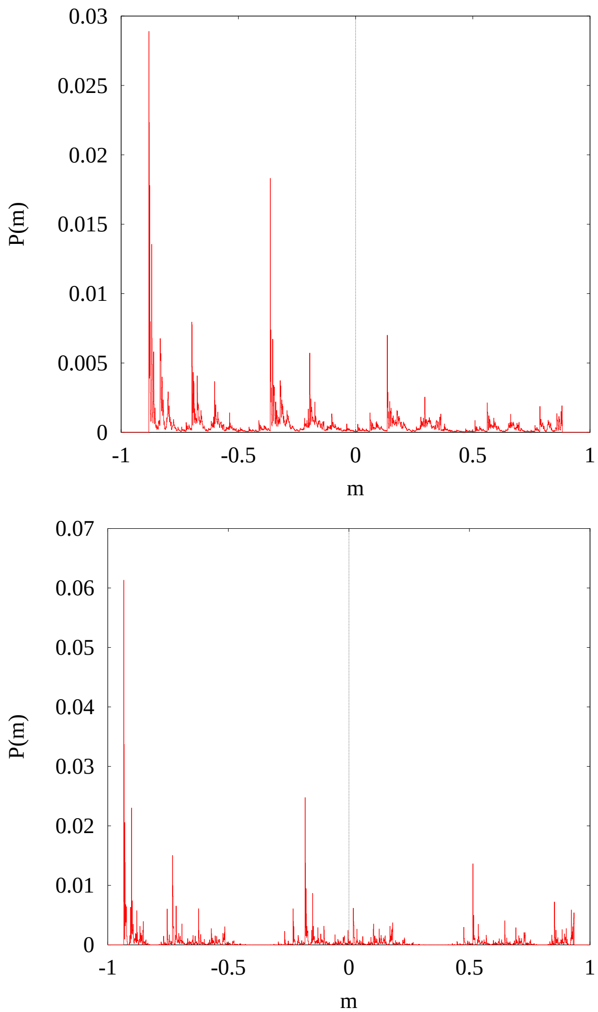

Figure 6.3: Population code of the mean field model with asymmetric driving field distribution, $p_+ = 0.4$. Top: Parameters are $K = 1.0$ and $\frac{H_0}{K} = 0.5$. Bottom: Parameters are $K = 1.0$ and $\frac{H_0}{K} = 0.75$.

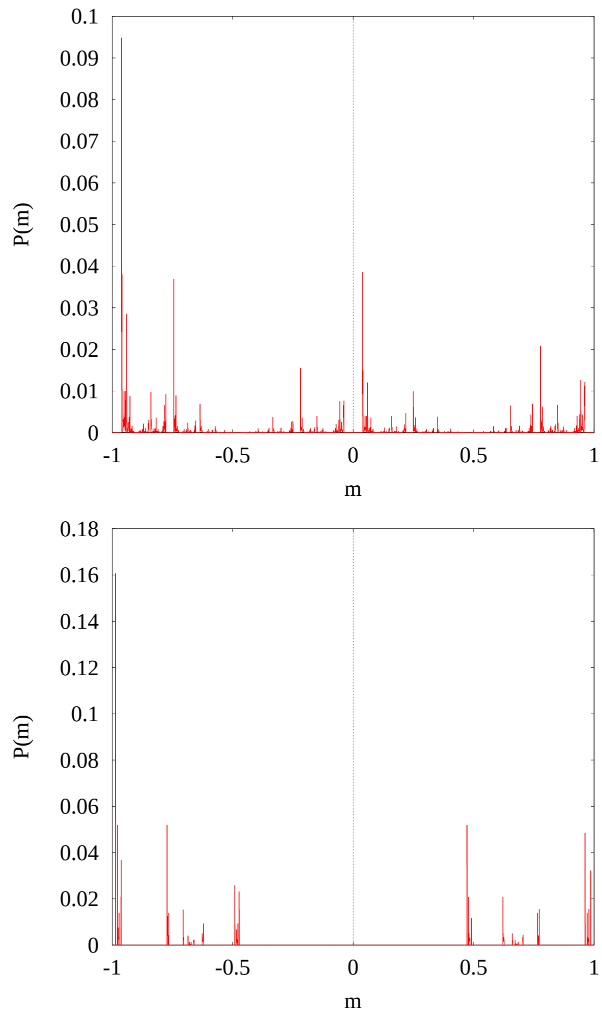

Figure 6.4: Same as Fig. 6.3. Top: Parameters are $K = 1.0$ and $\frac{H_0}{K} = 1.0$. Bottom: Parameters are $K = 1.0$ and $\frac{H_0}{K} = 1.5$.

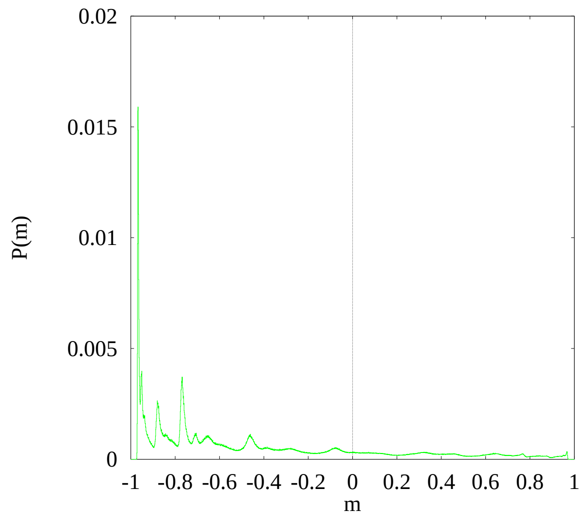

Figure 6.5: Population code from the two dimensional model with asymmetric driving field distribution, $p_+ = 0.4$. Parameters are $K = 1.0$ and $\frac{H_0}{K} = 1.0$.

fashion as in the mean field case, that is, one thousand mean field maps are tracked for five thousand iterations. In the cortical picture, they represent the average code distribution of one thousand *independent* cell assemblies, in which each neuron is connected to all others. The connectivity giving rise to supercolumns and clusters indicated in Fig. 6.2 is not taken into account here.

Similar structures may be seen in the two dimensional case, depicted in Figs. 6.5 and 6.6. Here, 64 systems of linear dimension $L = 143$ were simulated in parallel for close to 10^5 Monte Carlo steps, taking into account the new driving field distribution Eq. (6.1). Again, each system represents an independent cell assemblies, following a dynamics like that shown in Fig. 5.9 in the last chapter.

The neurobiological interpretation of the RDIM given in this chapter is only rudimentary. Yet, the focus on a strong, random external field leads to the observation that the distribution of the activity of a population of cells may have a complex, multifractal structure.

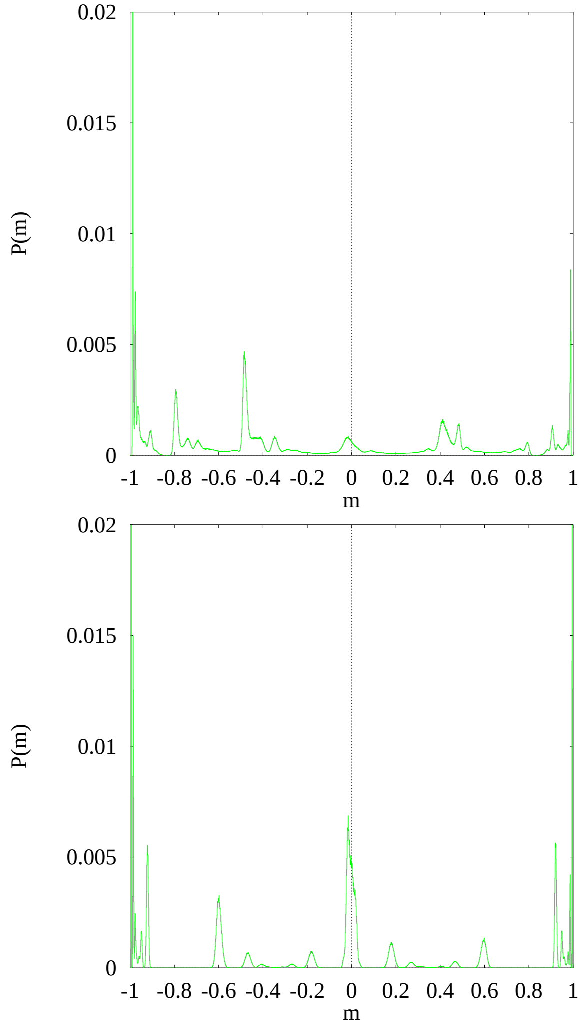

Figure 6.6: Two dimensional model with asymmetric driving field distribution, $p_+ = 0.4$. Top: Parameters are $K = 1.0$ and $\frac{H_0}{K} = 2.0$. Bottom: Parameters are $K = 1.0$ and $\frac{H_0}{K} = 3.0$. To focus on details of the structure, only $P(m) < 0.2$ is shown.

Chapter 7

Concluding remarks

To finish up this work, a short summary of results and several concluding remarks are in order. After introducing a formalism to describe strongly driven, nonequilibrium systems based on the Master Equation, the randomly driven Ising model (RDIM) was introduced and discussed as a prototype of such a system.

- The mean field RDIM was described by a stochastic map. The phase transition from para- to ferromagnetic behavior is first order. Below the equilibrium critical temperature, the magnetization jumps at a critical value of the driving field. This is due to dynamic freezing, which was discussed from a geometric point of view. The multifractal properties of the stationary magnetization distribution were revealed. Depending on temperature and driving field strength, they were categorized following [Ra93] as singular-continuous with fractal or euclidean support, or all-continuous. The phase transition does not depend on the dichotomic driving field, which may be replaced by any bounded continuous distribution.

- The one dimensional chain was solved only in part. Maps for the local magnetization and two spin correlation were constructed. Their translation invariant sectors may be solved, similar to the non-driven case [Gl63]. As expected, the phase transition occurs at $T_C = 0$, but again, only if the driving field is below a critical value. It was shown that the translation invariant magnetization map in the stationary state is a linear IFS, hence the support of the magnetization distribution is a

Cantor set. Its fractal dimension depends on both temperature and driving field strength.

Apart from the divergence of the relaxation time near $T_c = 0$, critical exponents were not investigated. Their analysis, and more specifically, their dependence on the form of the transition rate, could lead to further interesting results.

- The two dimensional RDIM cannot be solved analytically. Monte Carlo simulations performed on the neurocomputer SYNAPSE1/N110 indicate that the features seen in the mean field and one dimensional case survive the presence of thermal fluctuations. A rough phase diagram was derived from such simulations. Furthermore, the distributions of the mean magnetization show remnants of fractal behavior in both the para- and ferromagnetic phase.

  Here, a more detailed phase diagram would be of interest, especially with respect to finite size scaling. Also, a study of the dynamics of droplets and domain walls could prove to be worthwhile.

- The RDIM was interpreted as a primitive model of neural tissue. A spin was considered to be a neuron taking on the states "spike" or "no spike" and connectivity between cells was restricted to that of a ferromagnetic Ising model. In this view, the RDIM represents an assembly of cells with a common receptive field driven by external spikes. This situation occurs, for instance, in the primary visual cortex. One is led to the notion of population codes, the neurons passing information through their average state. The distribution of these codes is similar to the physical model's mean magnetization. In order to control the frequency of driving spikes, asymmetric driving field distributions may be employed.

  The neural picture was presented to draw attention to the fact that neurons may well be viewed as strongly driven statistical systems. Here, experimental evidence of RDIM-type behavior could be the incentive to move on to more realistic systems, including more complex connectivity patterns and, for instance, integrate-and-fire neurons.

Bibliography

[Gl63] R. J. Glauber, Time-dependent statistics of the Ising model, *J. Math. Phys.* **4** (1963) 294

[Ma77] B.B. Mandelbrot, The Fractal Geometry of Nature, W.H. Freeman & Co., New York (1977)

[Ru78] P. Ruján, Calculation of the free energy of Ising systems by a recursion method, *Physica A* **91** (1978) 549

[PoMa80] Y. Pomeau and P. Manneville, Intermittent transition to turbulence in dissipative dynamic systems, *Commun. Math. Phys.* **74** (1980) 189

[ChWr81] S-J. Chang and J. Wright, Transitions and distribution functions for chaotic systems, *Phys. Rev. A* **23** (1981) 1419

[AeBr83] G. Aeppli and R. Bruinsma, Linear response theory and the one-dimensional Ising ferromagnet in a random field, *Phys. Lett. A* **97** (1983) 117

[BrAe83] R. Bruinsma and G. Aeppli, One dimensional Ising model in a random field, *Phys. Rev. Lett.* **50** (1983) 1494

[HePr83] H.G.E. Henschel and I. Procaccia, The infinite number of generalized dimensions of fractals and strange attractors, *Physica D* **8** (1983) 435

[GyRu84] G. Györgyi and P. Ruján, Strange attractors in disordered systems, *J. Phys. C* **17** (1984) 4207

[BaDe85] M. F. Barnsley and S. Demko, Iterated function systems and the global construction of fractals, *Proc. R. Soc. Lond. A* **399** (1985) 243

[HaJe86] T.C. Halsey, M.H. Jensen, L.P. Kadanoff, I. Procaccia, B.I. Shraiman, Fractal measures and their singularities: The characterization of strange sets, *Phys. Rev. A* **33** (1986) 1141

[TaKo86] C. Tang and M. Kohmoto, Global scaling properties of the spectrum for a quasiperiodic Schrödinger equation, *Phys. Rev. B* **34** (1986) 2041

[Ts86] K. Y. Tsang, Dimensionality of strange attractors determined analytically, *Phys. Rev. Lett.* **57** (1986) 1390

[Ev87] S. N. Evangelou, Fractal measures in the random-field Ising model, *J. Phys. C* **20** (1987) L511

[SzBe87] P. Szépfalusy and U. Behn, Calculation of a characteristic fractal dimension in the one-dimensional random Ising model, *Z. Phys. B* **65** (1987) 337

[BeSz88] J. Bene and P. Szépfalusy, Multifractal properties in the one-dimensional random-field Ising model, *Phys. Rev. A* **37** (1988) 1703

[Sc88] H.G. Schuster, Deterministic Chaos, An Introduction, 2^{nd} Edition, VCH, Weinheim (1988)

[BaBr89] G. Bayreuther, P. Bruno, G. Lugert, and C. Turtur, Magnetic aftereffect in ultrathin ferromagnetic films, *Phys. Rev. B* **40** (1989) 7399

[Be89] J. Bene, Multifractal properties of a class of non-natural measures as an eigenvalue problem, *Phys. Rev. A* **39** (1989) 2090

[Ch89] S.S. Christensen et al, The primary visual system: An attempt to understand the function of its structure, In: Models of brain function, R.M.J. Cotterill, Ed., Cambridge University Press, Cambridge (1989), pp 199-209

[AlSt90] R. Allensbach, M. Stampanoni, and A. Bischof, Magnetic domains in thin epitaxial Co/Au(111) films, *Phys. Rev. Lett.* **65** (1990) 3344

[Fa90] K. Falconer, Fractal Geometry: Mathematical Foundations and Applications, John Wiley & Sons Ltd., Chichester (1990)

[LoPe90] W. S. Lo and R. A. Pelcovits, Ising model in a time-dependent magnetic field, *Phys. Rev. A* **42** (1990) 7471

[PoMe90] J. Pommier, P. Meyer, G. Pénissard, J. Ferré, P. Bruno, and D. Renard, Magnetization reversal in ultrathin ferromagnetic films with perpendicular anisotropy: domain observations, *Phys. Rev. Lett.* **65** (1990) 2054

[RaKr90] M. Rao, H. R. Krishnamurthy, and R. Pandit, Magnetic hysteresis in two spin systems, *Phys. Rev. B* **42** (1990) 856

[Re90] H. Reichert, Neurobiologie, Georg Thieme Verlag, Stuttgart (1990)

[ToOl90] T. Tomé and M. J. de Oliveira, Dynamic phase transition in the kinetic Ising model under a time-dependent oscillating field, *Phys. Rev. A* **41** (1990) 4251

[SeMa92] S. Sengupta, Y. Marathe, and S. Puri, Cell-dynamic simulation of magnetic hysteresis in two-dimensional Ising system, *Phys. Rev. B* **45** (1992) 7828

[HeWa93] Y.-L. He and G.-C. Wang, Observation of dynamic scaling of magnetic hysteresis in ultrathin ferromagnetic Fe/Au(001) films, *Phys. Rev. Lett.* **70** (1993) 2336

[Ra93] G. Radons, A new transition for projections of multifractal measures and random maps, *J. Stat. Phys.* **72**, 227 (1993)

[RiTo94] P. A. Rikvold, H. Tomita, S. Miyashita, and S. W. Sides, Metastable lifetimes in a kinetic Ising model: dependence on field and system size, *Phys. Rev. E* **49** (1994) 5080

[GaCo95a] G. Gallavotti and E. G. D. Cohen, Dynamical ensembles in nonequilibrium statistical mechanics, *Phys. Rev. Lett.* **74** (1995) 2694

[GaCo95b] G. Gallavotti and E. G. D. Cohen, Dynamical ensembles in stationary states, *J. Stat. Phys.* **80** (1995) 931

[SiRa96] S. W. Sides, R. A. Ramos, P. A. Rikvold, and M. A. Novotny, Response of kinetic Ising model system to oscillating external fields: Amplitude and frequency dependence, *J. Appl. Phys.* **79** (1996) 6482

[SiSz96] N. Simányi and D. Szász, The Boltzmann-Sinai hypothesis for hard ball systems, preprint, *mp-arcmath.utexas.edu - #96-80*

[HaRu97] J. Hausmann, P. Ruján, Stationary properties of a randomly driven Ising ferromagnet, *Phys. Rev. Lett.* **79** (1997) 3339

[Ac98] M. Acharrya, Nonequilibrium phase transition in the kinetic Ising model: Dynamical symmetry breaking by randomly varying magnetic field, *Phys. Rev. E* **58** (1998) 174

[HaRu99a] J. Hausmann, P. Ruján, The randomly driven Ising ferromagnet: I. General formalism and mean field theory, *J. Phys. A* **32** (1999) 61

[HaRu99b] J. Hausmann, P. Ruján, The randomly driven Ising ferromagnet: II. One and two dimensions, *J. Phys. A* **32** (1999) 75

Lebenslauf

Name: Johannes Hausmann
Geboren am: 10. April 1968 in Freiburg i.Br.
Familienstand: Ledig.

Ausbildung

- 74-78: Grundschule in Freiburg i.Br.
- 78-81: International School of Belgrade, Jugoslawien
- 81-82: Hommocks Middle School in Mamaroneck, NY, U.S.A.
- 82-84: Mamaroneck High School in Mamaroneck, NY, U.S.A.
- 84-87: Theodor-Heuss-Gymnasium in Freiburg i.Br., Abschluß Abitur.
- 87-90: Studium der Physik Albert-Ludwigs-Universität Freiburg, Vordiplom.
- 90-95: Studium der Physik Carl-von-Ossietzky-Universität Oldenburg, Abschluß Diplom.
- 95-99: Wissenschaftlicher Mitarbeiter der AG Sp$\hat{\mathrm{I}}$n am FB Physik der Carl-von-Ossietzky-Universität Oldenburg.

Oldenburg, den 16. 10. 2001

Erklärung

Hiermit versichere ich, daß ich diese Arbeit selbständig verfaßt und keine anderen als die angegebenen Hilfsmittel verwendet habe.

(Johannes Hausmann)